NATIONAL TRANSPORTATION SAFETY BOARD
Office of Research and Engineering
Materials Laboratory Division
Washington, D.C. 20594

March 15, 2019

MATERIALS LABORATORY FACTUAL REPORT Report No. 18-061

A. ACCIDENT INFORMATION

Place	:	Daytona Beach, Florida
Date	:	April 4, 2018
Vehicle	:	Piper PA-28R-201, N106ER
NTSB No.	:	ERA18FA120
Investigator	:	Aaron McCarter, AS-ERA / Clinton R. Crookshanks, AS-40

B. COMPONENTS EXAMINED

Center wing box assembly and left and right wing main spar pieces from N106ER, left wing main spar piece from N104ER, right wing main spar piece from N3986M, and 3 new spar extrusions.

C. DETAILS OF THE EXAMINATION

Overall views of the submitted center wing box assembly with attached right wing main spar piece and fractured left wing main spar piece are shown in figure 1. The right main spar was cracked at the inboard attachment location and the outboard end of the piece was deflected forward. The left main spar was fractured at the inboard attachment location. A group examination of the components was conducted on April 10 through 12, 2018 at the NTSB Materials laboratory with Structures Group representatives from the NTSB, Federal Aviation Administration, Piper Aircraft, Inc., and Embry-Riddle Aeronautical University (ERAU) present.

1. Accident Airplane Main Wing Spars

At the time of the accident, the airplane had accrued 7,690.6 hours time in service (TIS). The airplane, serial number 2844137, had been operated by ERAU since it was manufactured in 2007 and had always been used for certified flight instructor and commercial pilot training. The total landing cycles at the time of the accident were 33,276 based on ERAU information documented in their Education and Training Administration program.

According to engineering drawings for the accident airplane, the main spar is an I-shaped extrusion of aluminum alloy 2024-T3511. As installed on the airplane, each wing spar is attached to the center wing box with 18 attachment bolts; 8 through the upper spar cap and 10 through the lower spar cap. In each spar cap, half of the bolts are located in a line forward of the spar web, and the remaining bolts are located in a line aft of the web.

Doublers are riveted to the forward and aft sides of the spar at the attachment location and outboard beyond the bend in the spar that forms the wing dihedral. Flanges for the doublers extend over the upper and lower spar caps at the forward side of the spar and over the lower spar cap at the aft side of the spar.

For reference in this report, wing spar attachment bolts were labeled with three alphanumeric characters to identify their locations. The first letter in the identification was an L or an R, indicating left or right wing, respectively. The second letter in the identification indicated the row of bolts consistent with the labeling method used in the Piper Aircraft, Inc. PA-28R-201 Arrow Maintenance Manual. Attachment locations for the upper spar cap were identified with A and B, where row A was located forward of the spar web and row B was located aft of the web. Attachment locations for the lower spar cap were identified with C and D, where row C was located forward of the spar web and row D was located aft of the web. Finally, the bolts in each row were identified with a number in sequence starting from the outboard bolt, also consistent with the labeling method used in the aircraft maintenance manual. As in the manual, a dash is inserted between the row letter and the number. As an example, the outboard attachment bolt in the lower spar cap forward of the web in the left wing would be labeled LC-1.

Views of the fracture in the left spar are shown in figures 2 and 3. The lower spar cap shown in figures 2 and 3 had a fracture that intersected holes for attachment bolts LC-1 and LD-1. Portions of the fracture surface had relatively smooth features in a plane perpendicular to the longitudinal axis, features consistent with fatigue fracture. Crack arrest lines were visible on the fracture surfaces of the lower spar cap and the forward and aft doublers, also consistent with fatigue fracture. Some of the fracture features were obscured by black-colored deposits, particularly in the areas near the apparent fatigue origins. The upper spar cap displayed rough matte-gray features consistent with ductile overstress fracture. Deformation associated with the fracture in the upper spar cap was consistent with an upward bending load.

The outboard side of the fracture shown in figure 3 was cut from the rest of the spar to facilitate further examination. Additionally, the forward and aft doublers were removed from the sectioned piece by drilling out several rivets. To remove the black deposits from the surface, acetate replica tape was applied to the surface and removed after drying. After several applications of the replica tape, the pieces were placed in a bath of acetone and cleaned using an ultrasonic cleaner. A view of the lower spar cap and doubler pieces after sectioning, separating, and cleaning is shown in figure 4 with closer views in figure 5.

Unlabeled arrows in figure 5 indicate locations of fatigue origins, and dashed lines indicate fatigue boundaries. In the lower spar cap, origins were located at the lower surface both forward and aft of hole LC-1 and at the aft side of hole LD-1. Forward of hole LC-1, fatigue features extended to the forward edge of the lower spar cap as shown in a closer view of the fracture surface in figure 6. Aft of hole LC-1, fatigue features extended aft through the spar cap, intersecting the lower side of hole LD-1, and upward into the web to the boundary located approximately 0.75 inch above the spar cap. From

the aft side of hole LD-1, fatigue features extended to the boundary near the upper aft side of the lower spar cap as shown.

Closer views of the fatigue region aft of hole LC-1 are shown in figure 7. Near the surfaces of the spar cap, fatigue features had a different texture, appearing smoother than features near the middle of the thickness with a distinct boundary between the different-textured regions. Brackets in figure 7 indicate smoother areas at the lower surface of the spar cap.

In the doublers, fatigue origins were noted on the lower sides of the doublers both forward and aft of the attachment holes. The fatigue region in the forward doubler was larger, extending forward to the forward edge of the doubler and upward approximately 1.25 inches from the aft side of the hole. In the aft doubler, the fatigue regions extended to the boundaries shown in figure 5 where the boundaries were approximately 7/8 inch apart.

Next, the lower spar cap was examined using a scanning electron microscope (SEM). Parts of the fracture surface remained obscured by light green deposits on the surface visible in the optical image in figure 6. The deposits generally appeared brighter in the SEM due to charging effects associated with SEM imaging of nonconductive materials.

SEM views of the origin areas at the forward and aft sides of hole LC-1 are shown in figures 8 and 9. Unlabeled arrows in figures 8 and 9 indicate local directions of fatigue crack propagation based on available fracture features in the images. The origin areas in each location appeared partly obscured or damaged by post-fracture rubbing or deposits on the surface. However, fracture features appeared to emanate from origins at the lower surface of the spar cap adjacent to attachment hole LC-1.

To further characterize the origin areas at the forward and aft sides of hole LC-1 on the lower spar cap, the fracture surface was cleaned by briefly submerging the piece with the fracture surface in a heated aqueous solution containing phosphoric acid and chromium trioxide. A photograph of the fracture surface after completion of the chemical cleaning process is shown in figure 10.

SEM images of the chemically cleaned origin areas at the forward and aft sides of hole LC-1 are shown in figures 11 and 12, respectively. After cleaning, deposits that partly obscured the origin areas were removed, revealing additional fracture features. At the forward side of hole LC-1, fracture features at the corner between hole LC-1 and the lower surface appeared rubbed. However, the direction of local crack propagation in adjacent areas of the fracture surface (see unlabeled arrows in figure 11) appeared to be consistent with a crack origin at the lower surface adjacent to hole LC-1. At the aft side of the hole shown in the upper image in figure 12, a deformed lip was present on the lower side of the fracture which obscured fracture features at the lower edge, and the fracture surface appeared deformed along the edge of hole LC-1 near the lower surface.

To further characterize the origin area at the aft side of hole LC-1, a transverse cut was made through the left wing main spar lower spar cap approximately 1 inch inboard of the fracture to facilitate an SEM examination of the mating (inboard) fracture surface. After sectioning, the fracture surface was cleaned with acetone followed by application and removal of acetate tape to lift off surface deposits. Next, the piece with the fracture surface was cleaned using the chemical method applied to the mating side of the fracture described above. A view of the origin area at the aft side of hole LC-1 after chemical cleaning is shown in the lower image in figure 12. A bracket in figure 12 indicates a fatigue origin area located in the chamfer between the lower surface and hole LC-1. Unlabeled arrows in the lower image in figure 12 indicate the local crack propagation directions emanating from the indicated origin area.

A section of the left wing main spar lower spar cap was cut from the outboard end of the piece shown in figure 4 to facilitate a metallographic examination. The spar cap piece was mounted in epoxy, polished, and etched by immersion in Keller's reagent. A macrograph of the etched cross-section is shown in figure 13. The microstructure in the spar cap consisted of large surface grains surrounding a finer-grain core. Micrographs of the cross-section at the lower surface are shown in figure 14.

Hardness and conductivity were measured on pieces of the left wing main spar lower spar cap. The average hardness measured 81.0 HRBW, an average of 5 measurements from the middle of the spar cap cross-section on the mounted sample shown in figure 13. According to the ASM Handbook,[1] the typical hardness of aluminum alloy 2024-T351 is 76 HRB (120 HB). Paint was removed from an area of the spar cap to facilitate a conductivity measurement on the surface of the spar cap. The conductivity measured 29.3% IACS. According to the ASM Handbook, the typical conductivity for aluminum alloy 2024-T351 is 30% IACS. The thickness of the left wing main spar lower spar cap measured 0.270 inch, which was within the allowable thickness range specified in the engineering drawing.

The fracture features on the cracked right spar were partially visible, but further disassembly, including removing the bolts attaching the spar piece to the center box assembly, was required to facilitate a detailed examination of the fracture features. Before removing the bolts, the bolts were examined, and then torque measurements were made on each bolt. The torque stripes on the heads and nuts of the bolts were intact with no evidence of movement. Each bolt had 1 washer under the head, and bolts RC-1, RC-5, RD-1, RD-5, LC-1, LC-5, LD-1, and LD-5 each had one washer under the nut. The remaining bolts had 2 washers under the nut. According to the Piper Aircraft Maintenance Manual, the main spar attachment bolts should have 1 washer under the head and at least 1 washer under the nut.

Torque required to move the nut was measured on each of the attachment bolts. For bolt RA-4, the torque was initially measured in the tightening direction, where the measured torque was 17 foot-pounds. The loosening torque required for first movement

[1] ASM Handbook Volume 2: Properties and Selection: Nonferrous Alloys and Special Purpose Materials, ASM International (1990).

was then measured at 19 foot-pounds. For the remaining measurements, the torque was only measured in the loosening direction. On bolts RA-1, RA-2, and RA-3, the position of the nuts were marked, the torque required to return the nut to its original position was also recorded. For bolts RA-1, RA-2, and RA-3, the movement torque in the loosening direction was 11.9 pound-force feet, 17.0 pound-force feet, and 22.4 pound-force feet, respectively. The torque to return to the original position measured 15.3 pound-force feet, 16.0 pound-force feet, and 21.8 pound-force feet, respectively. First movement torque measurements in the loosening direction for each of the attachment bolts is listed in table 1. According to the Piper Aircraft Maintenance Manual, the installation torque to be applied to the upper spar cap bolt heads and the lower spar cap nuts is 30 pound-force feet to 32.5 pound-force feet (360 pound-force inches to 390 pound-force inches).

After torque measurements were completed, the right main spar piece was disassembled from the center wing box assembly, and cuts were made to facilitate separating the mating fracture surfaces. Views of the inboard side of the fracture after completing the break with a lab fracture is shown in figure 15. The fracture surface had mostly rough matte-gray features consistent with ductile overstress fracture. River patterns associated with the fracture emanated from hole RD-1 located aft of the spar web consistent with fracture initiation near hole RD-1. The overstress fracture in the right main spar lower spar cap emanated forward, intersecting hole RC-1. As shown in figure 15, a reflective area was observed on the fracture surface at the lower aft side of hole RC-1.

The right wing main spar lower spar cap piece shown in figure 15 was further examined using an SEM, and resulting images of the reflective area at the forward side of hole RC-1 are shown in figure 16. At higher magnification, striations were observed consistent with fatigue. Fatigue features emanated from an origin area located at the hole surface as indicated with a bracket in the lower image in figure 16. A dashed line in the upper image in figure 16 indicates the fatigue boundary, extending up to 0.047 inch aft of the hole and 0.038 inch upward from the lower surface. Where the fatigue region intersected the lower surface, the fatigue crack length was 0.026 inch. No evidence of a preexisting crack was observed at hole RD-1 (where the overstress fracture of the spar cap initiated).

The overstress fracture at the forward side of the hole was located outboard of the transverse plane intersecting the hole center. A tilted view of the forward edge of the hole inboard of the overstress fracture is shown in the upper image in figure 17. As indicated, a crack was observed at the forward edge of the hole where it intersected the lower surface. A closer view of the crack fracture surface is shown in the lower image in figure 17. Smooth fracture features with curving crack arrest lines were observed consistent with fatigue fracture. Ratchet marks[2] were also observed, consistent with multiple fatigue origins. A bracket in the lower image in figure 17 indicates the fatigue origin area located in the chamfer between the hole bore and the lower surface of the main spar.

[2] A ratchet mark is a small step in the fracture surface formed when two adjacent fatigue cracks originate on slightly offset planes.

Table 1. Loosening Torque Measurements

Attachment Bolt Identification	Torque (pound-force feet)	Attachment Bolt Identification	Torque (pound-force feet)
RA-1	11.9	**RC-1**	<5.0
RA-2	17.0	**RC-2**	19.0
RA-3	22.4	**RC-3**	23.9
RA-4	19.7*	**RC-4**	29.2
RB-1	10.0	**RC-5**	<5.0
RB-2	21.0	**RD-1**	<5.0
RB-3	17.8	**RD-2**	9.5
RB-4	17.7	**RD-3**	10.7
LA-1	5.1	**RD-4**	10.9
LA-2	11.8	**RD-5**	5.8
LA-3	14.6	**LC-1**	8.3
LA-4	9.9	**LC-2**	19.5
LB-1	8.3	**LC-3**	21.0
LB-2	20.4	**LC-4**	21.9
LB-3	26.0	**LC-5**	10.0
LB-4	23.8	**LD-1**	9.3
		LD-2	17.9
		LD-3	19.7
		LD-4	23.5
		LD-5	8.9

*After movement had been detected with tightening torque applied.

A piece of the main spar cap from the left wing was sent to Lehigh Testing Laboratories, Inc., New Castle, Delaware, for tension testing and chemical analysis. The sent piece was an approximately 10.5 inches long section of the lower spar cap with the web cut nearly flush to the upper surface of the spar cap. To prepare the piece for shipment to the test lab, rivets attaching the wing lower skin were drilled out to separate the skin from the spar cap. Then the piece was soaked in paint stripper to chemically remove the paint in preparation for machining of tensile specimens.

At Lehigh Testing, four subsize tensile specimens were machined from the lower spar cap from the middle portion between the rivet holes and outboard attachment bolt holes. Additional machining was required on the upper face to reduce the tensile specimen thickness to within tension specimen standard dimensions in accordance with ASTM Standard E8/E8M.[3] The lower surface remained in the as-received condition on the tensile specimens.

[3] ASTM E8/E8M – 16a, *Standard Test Methods for Tension Testing of Metallic Materials*, ASTM International (2016).

Results of the tension tests and chemical analysis are presented in Appendix A. The average yield strength (0.2% offset method), tensile strength, and elongation (in 1 inch) for the 4 samples was 64,000 psi, 86,500 psi, and 18.5%, respectively. The yield strength, tensile strength, and elongation for each of the tension specimens conformed to the requirements listed in SAE AMS specification QQ-A-200/3F,[4] the materials specification listed on the engineering drawing for the main spar extrusion. The chemical composition of the wing main spar material also conformed to the requirements listed in SAE AMS specification QQ-A-200/3F.

2. Airplane N104ER Left Main Wing Spar

An eddy current inspection of the wing spars from airplane N104ER, serial number 2844135, was conducted following the accident. A crack indication was detected at the forward side of the left wing spar attachment hole LC-1. Airplane N104ER had also been operated by ERAU since it was manufactured in 2007 and had accrued 7,660.7 hours TIS and 32,288 landing cycles.

The inboard end of the wing spar was separated from the rest of the wing and sent to the NTSB Materials Laboratory for examination, and a view of the submitted piece is shown in figure 18. A crack feature was visible under optical magnification as shown in figure 19, where a bracket indicates the location of a crack feature extending from the forward side of hole LC-1. No crack features were detected under optical magnification at the aft side of hole LC-1.

Next, the wing spar was cut to facilitate opening the crack by lab fracture. A transverse cut was made inboard of the attachment holes followed by a longitudinal horizontal cut through the web above the lower spar cap to separate the lower spar cap from the rest of the piece. Then a vertical cut was made through the row C attachment holes followed by a transverse cut through the forward edge of the lower spar cap toward the crack tip. The sectioned piece was then bent by hand to open the crack shown in figure 19.

After an initial examination under an optical stereomicroscope, the lab fracture was placed in the SEM for further examination. The crack fracture surface exposed by the lab fracture had relatively smooth features with curving crack arrest lines, features consistent with fatigue. A dashed line in figure 20 indicates the extent of the fatigue region extending up to 0.126 inch forward from the hole surface and up to 0.115 inch upward from the lower surface. Where the fatigue region intersected the lower surface, the length from the hole surface to the fatigue boundary was 0.119 inch.

A closer view of the fatigue origin area is shown in the lower image in figure 20. Ratchet marks were observed indicating multiple fatigue origins within the area indicated by the unlabeled bracket. The origins were located within the corner radius between the hole LC-1 bore and main spar lower surface.

[4] SAE AMS-QQ-A-200/3, *Aluminum Alloy 2024, Bar, Rod, Shapes, Tube, and Wire, Extruded*, SAE International (1997).

A transverse cut was made to separate a piece of the lower spar cap from the outboard end of the main spar piece shown in figure 18 for metallographic examination. The spar cap piece was mounted in epoxy, polished, and etched by immersion in Keller's reagent. A macrograph of the etched cross-section is shown in figure 21. The microstructure in the spar cap consisted of large surface grains surrounding a finer-grain core. Micrographs of the cross-section at the lower surface are shown in figure 22.

Hardness and conductivity measurements were made on the lower spar cap of the left main wing spar. The average hardness measured 80.8 HRBW, averaged from 5 measurements at the middle of the spar cap cross-section shown in figure 21. Conductivity measured on the lower surface of the spar was 29.8% IACS.

3. Airplane N3986M Right Main Wing Spar

The inboard end of the right wing spar from retired airplane N3986M, serial number 28R-7837150, was sent to the NTSB Materials Laboratory from another flight school in Florida for examination. The airplane had been manufactured in 1978, and reportedly had 9,841.3 hours TIS. The attachment bolt holes in the main spar were inspected using eddy current inspection, and no crack indications were detected. The lower surface around attachment holes RC-1 and RD-1 were examined under optical magnification, and no crack features were detected.

A transverse cut was made to separate a piece of the lower spar cap from the outboard end of the submitted main spar piece (see figure 23) for metallographic examination. The spar cap piece was mounted in epoxy, polished, and etched by immersion in Keller's reagent. A macrograph of the etched cross-section is shown in figure 24. The microstructure in the spar cap consisted of large surface grains surrounding a finer-grain core. Micrographs of the cross-section at the lower surface are shown in figure 25.

Hardness and conductivity measurements were made on the lower spar cap of the left main wing spar. The average hardness measured 79.9 HRBW, averaged from 5 measurements at the middle of the spar cap cross-section shown in figure 21. Conductivity measured on the lower surface of the spar was 29.7% IACS.

4. New Wing Main Spar Pieces

Piper Aircraft provided pieces from three different lots of recently purchased main spar extrusions for examination. The pieces were also supplied with their associated extrusion mill certificate of conformance documents. According to data supplied on the conformance certificates, testing from each lot showed the material satisfied the requirements for chemical composition, yield strength, tensile strength, and elongation as required in SAE AMS specification QQ-A-200/3F.

An overall view of the submitted new main spar extrusion pieces are shown in figure 26. For reference the pieces were received numbered 1 through 3 as shown in figure 26. A piece of the lower spar cap was cut from each sample for metallographic

examination. The spar cap pieces from new spars 1 and 2 were mounted in one epoxy form for convenience, and new spar 3 was mounted in a separate epoxy form. The mounted samples were polished and etched by immersion in Keller's reagent. Macrographs of the etched cross-sections are shown in figures 27 and 28. The microstructure in spar caps consisted of large surface grains surrounding a finer-grain core. Micrographs of the new spar 1 cross-section shown in figure 29 represent the typical microstructure observed on the new spar caps.

Hardness and conductivity measurements were made on the lower spar caps of each new spar piece. The average hardness measured 80.0 HRBW, 80.4 HRBW, and 80.0 HRBW on new spar pieces 1, 2, and 3, respectively. The average hardness value for each spar was calculated from 5 measurements at the middle of the spar cap cross-sections shown in figures 27 and 28. Each of the new spar pieces had the same value for conductivity (29.8% IACS) measured on the lower surface of each spar.

Matthew R. Fox, Ph.D.
Senior Materials Engineer

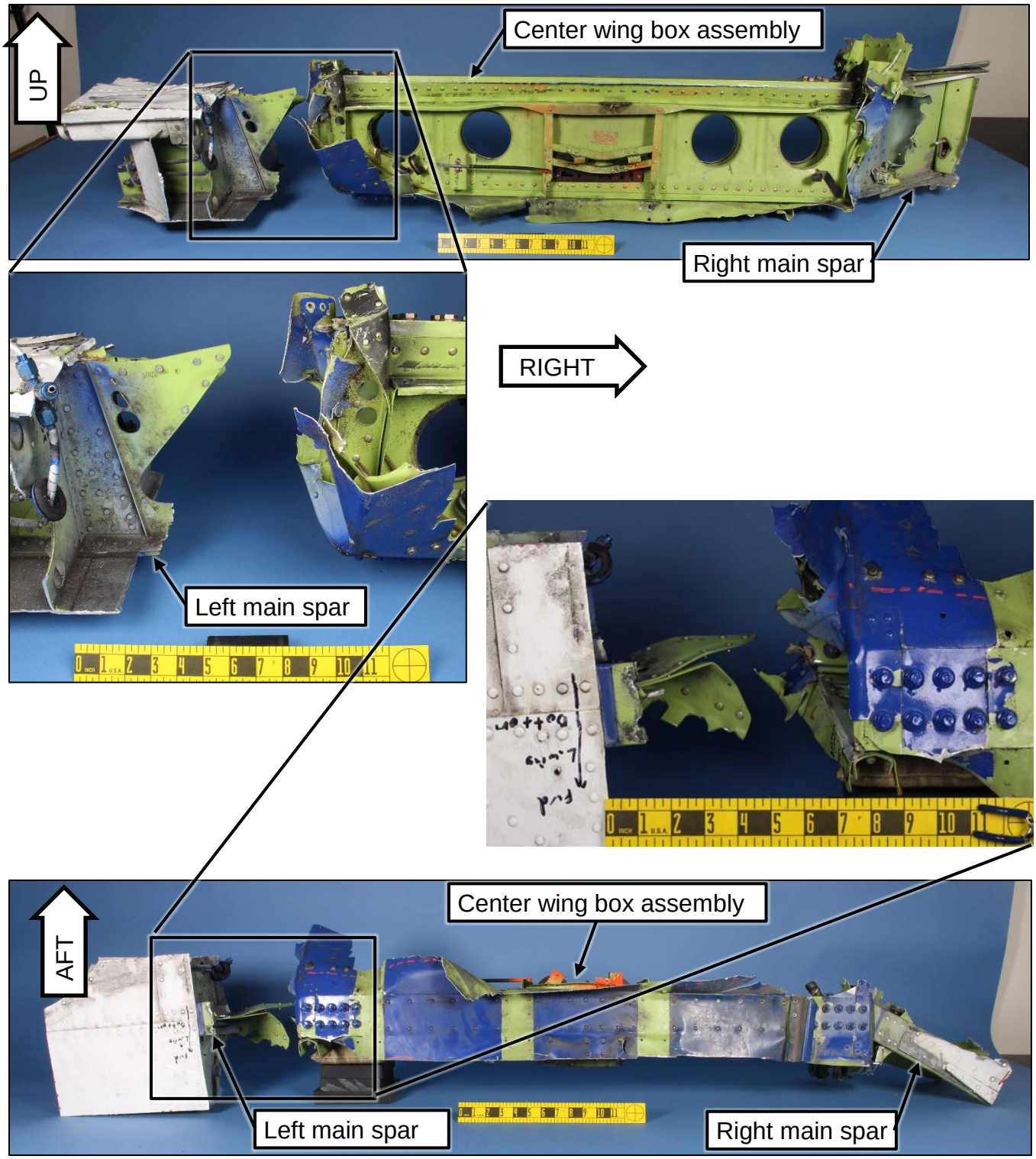

Figure 1. Overall views of the submitted components from the accident airplane showing the aft (upper images) and lower (lower images) surfaces.

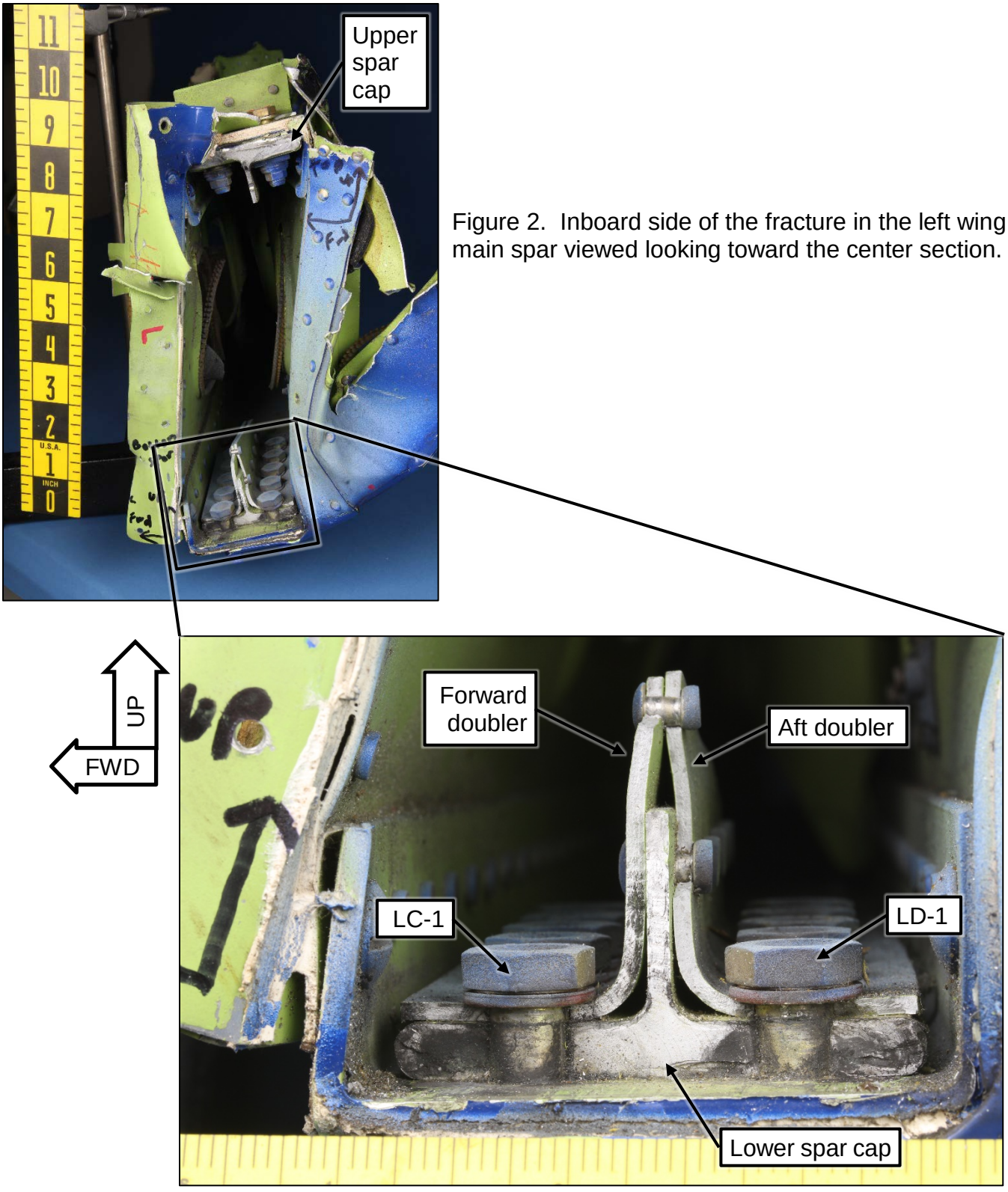

Figure 2. Inboard side of the fracture in the left wing main spar viewed looking toward the center section.

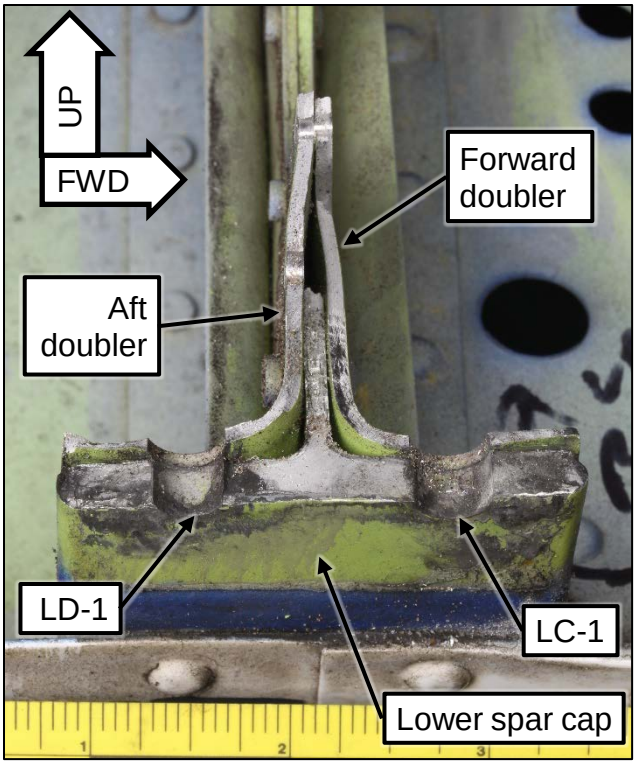

Figure 3. Outboard side of the fracture in the lower spar cap and attached doublers of the left wing main spar.

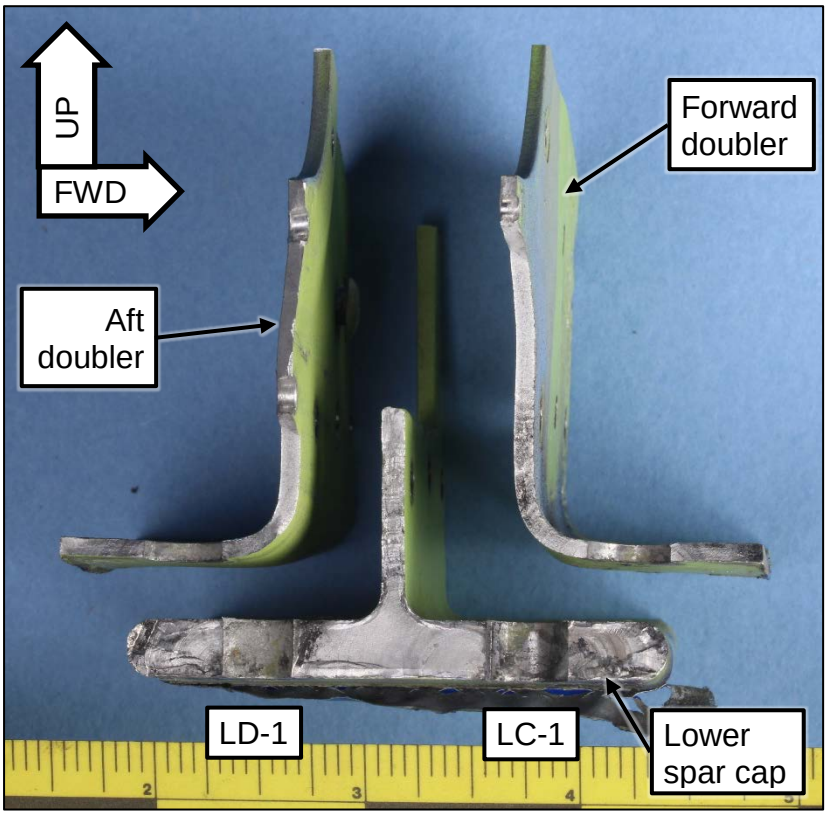

Figure 4. Pieces of the left wing lower spar cap and doublers shown in figure 3 after sectioning and removing rivets to facilitate examination of the fracture surfaces. The surfaces were also cleaned using acetate tape and acetone.

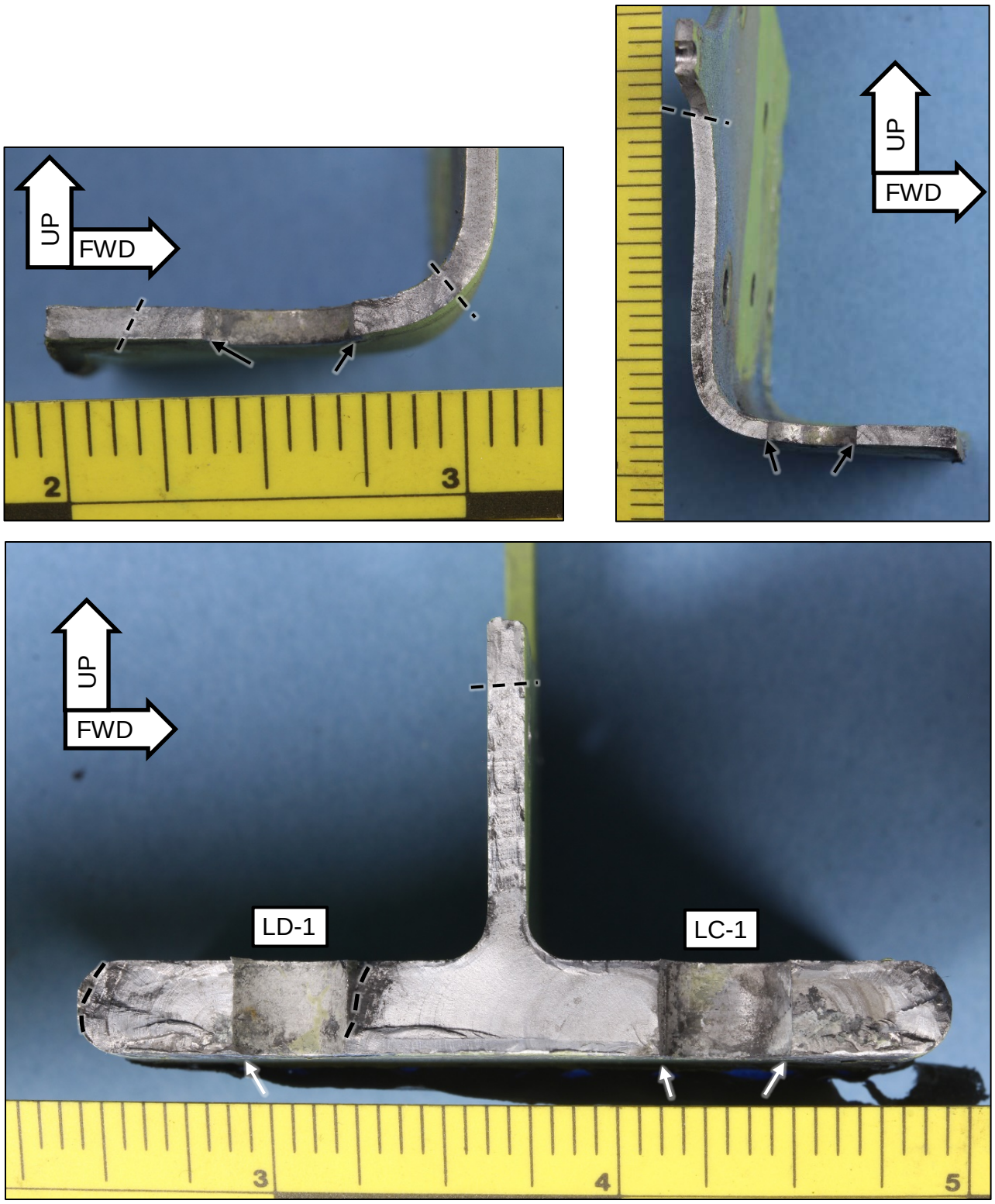

Figure 5. Closer views of the fracture surfaces in the doublers (upper images) and the lower spar cap (lower image) after cleaning. Unlabeled arrows indicate fatigue origin areas, and dashed lines indicate fatigue boundaries.

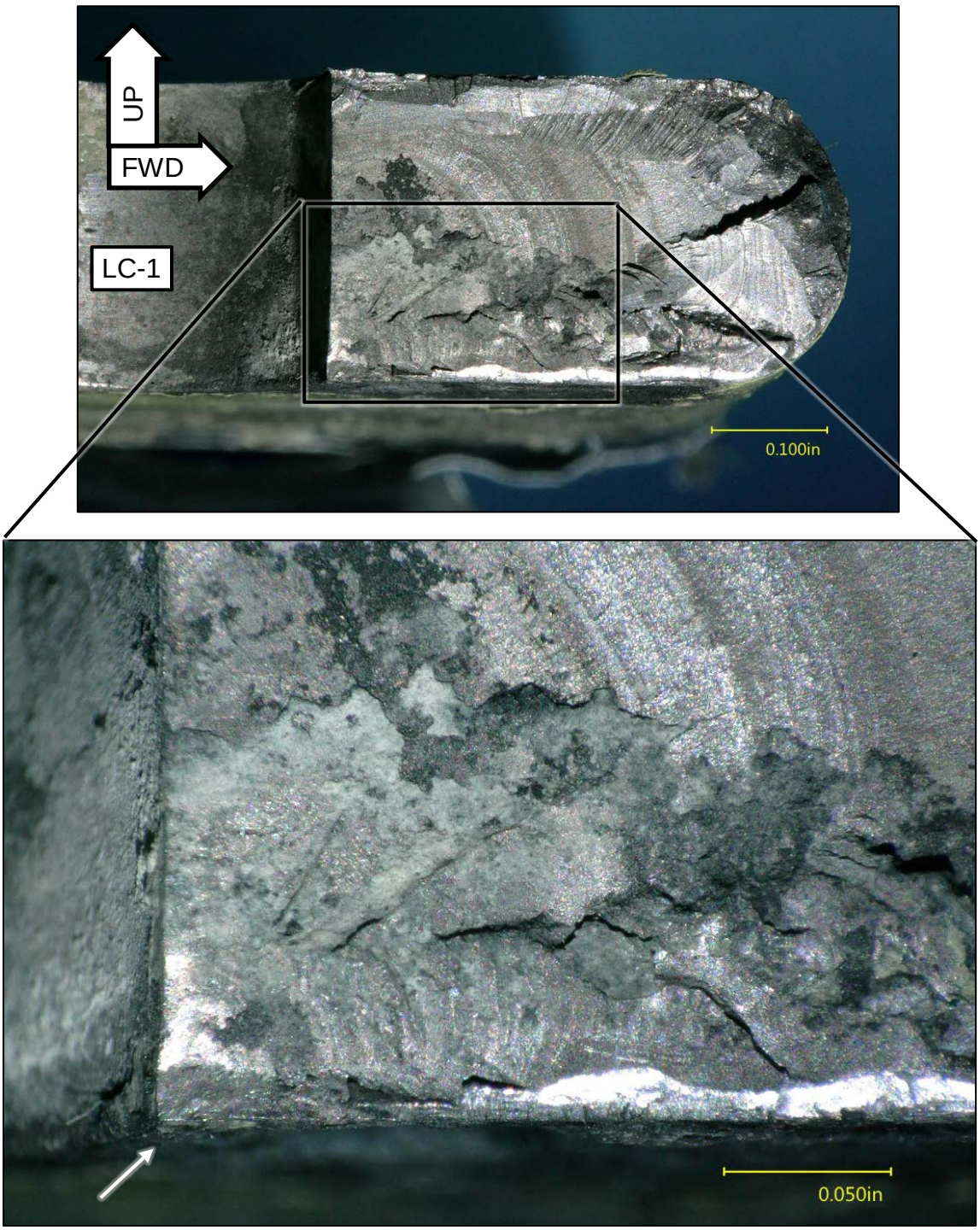

Figure 6. Optical images of the fatigue region forward of hole LC-1 (upper image) with a closer view of the fatigue origin area. An unlabeled arrow indicates the fatigue origin area.

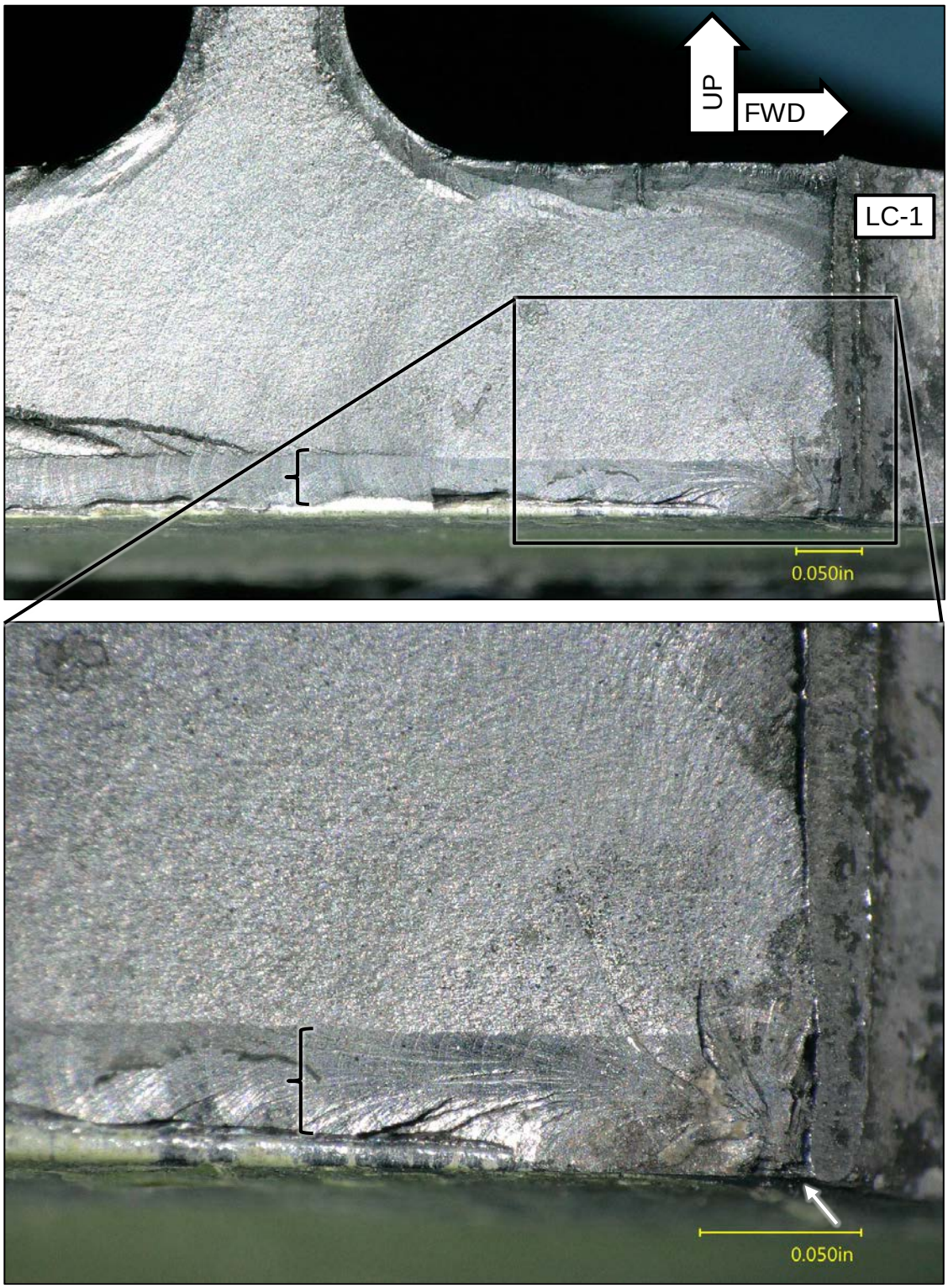

Figure 7. Optical images of fatigue features aft of hole LC-1 including a view of the origin area at higher magnification (lower image). Unlabeled brackets indicate areas near the surface with relatively smoother fatigue features, and an unlabeled arrow indicates the fatigue origin area.

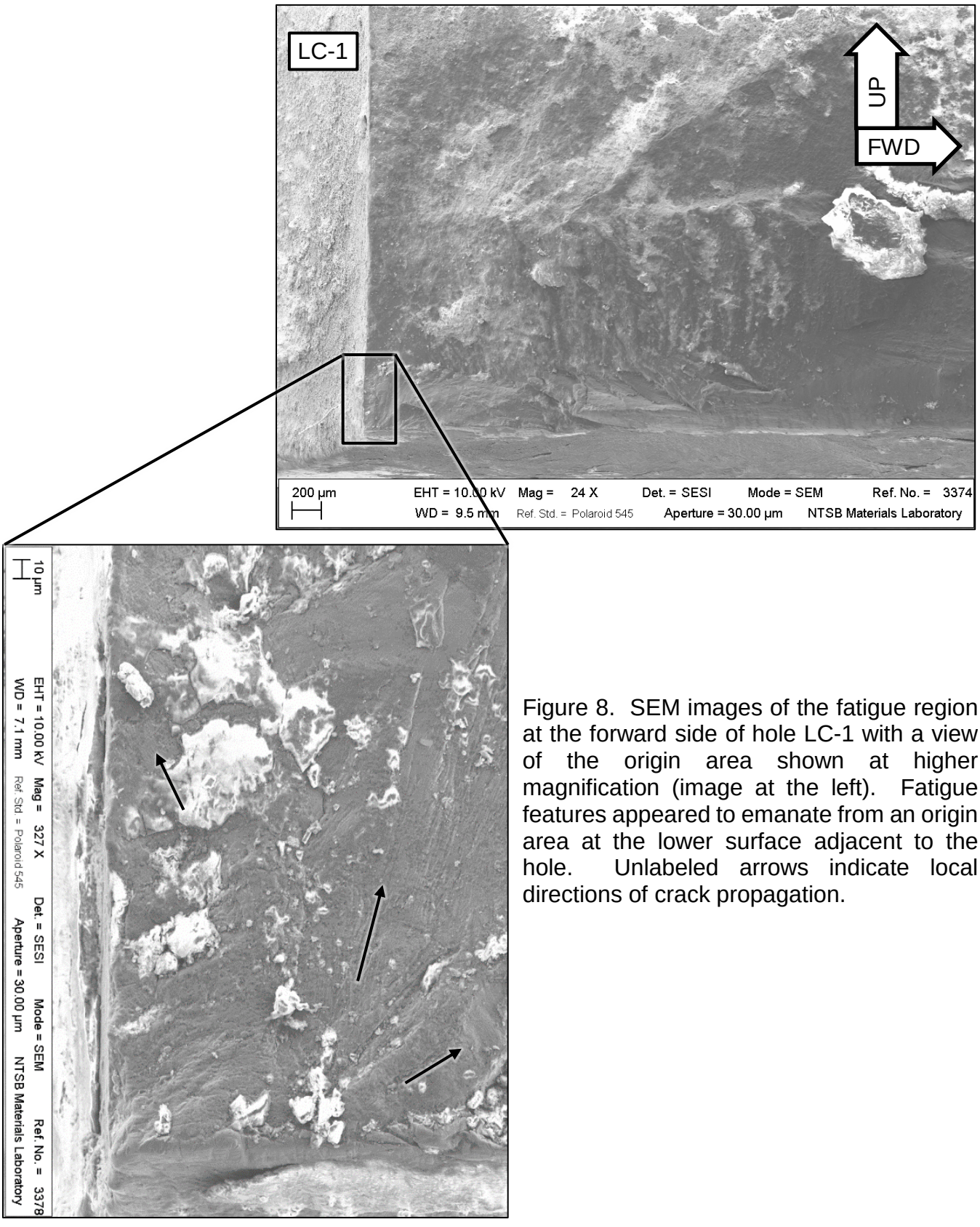

Figure 8. SEM images of the fatigue region at the forward side of hole LC-1 with a view of the origin area shown at higher magnification (image at the left). Fatigue features appeared to emanate from an origin area at the lower surface adjacent to the hole. Unlabeled arrows indicate local directions of crack propagation.

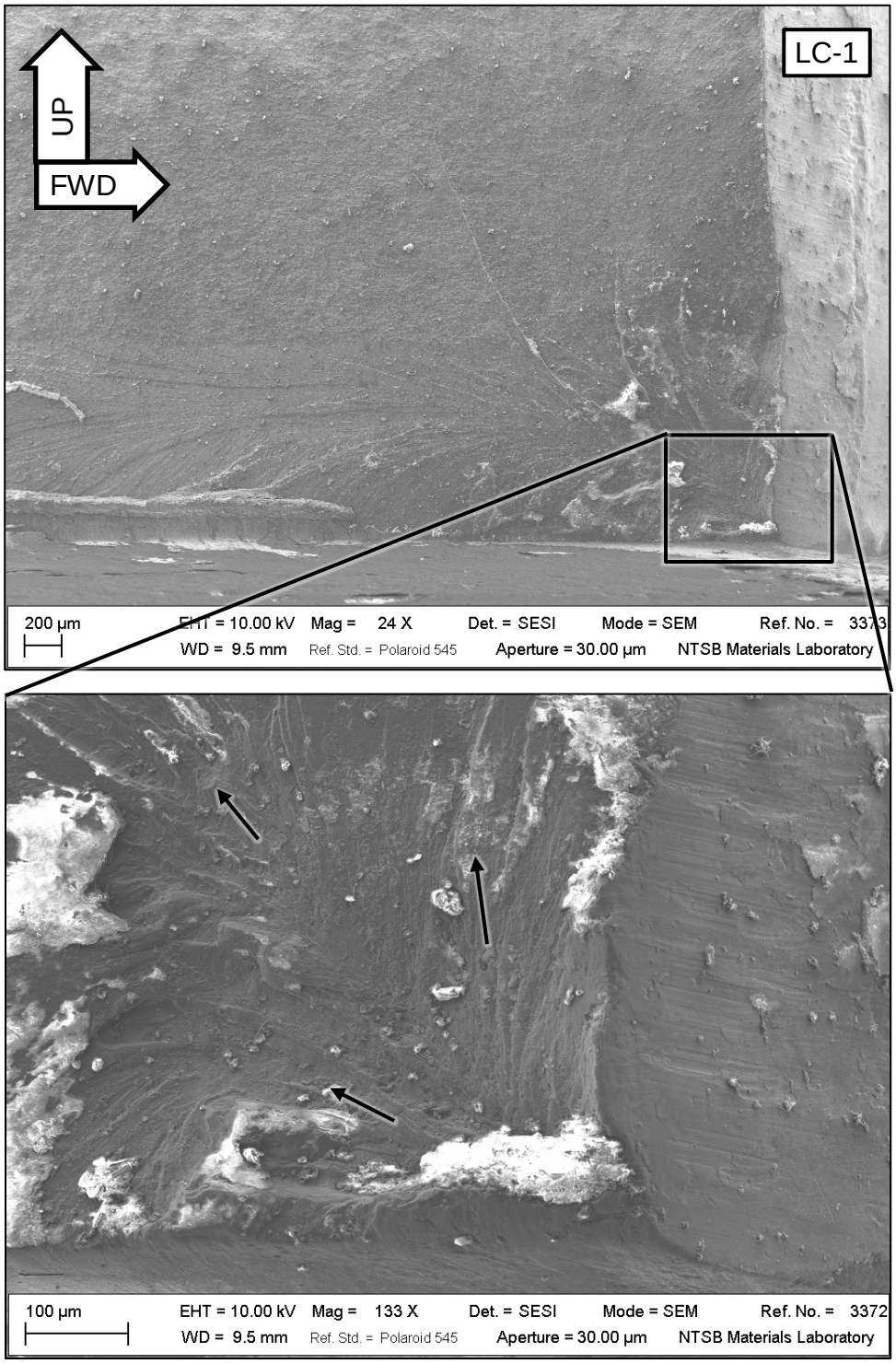

Figure 9. SEM images of fracture features at the aft side of hole LC-1 with a view of the origin area shown at higher magnification (lower image). Unlabeled arrows indicate local directions of crack propagation.

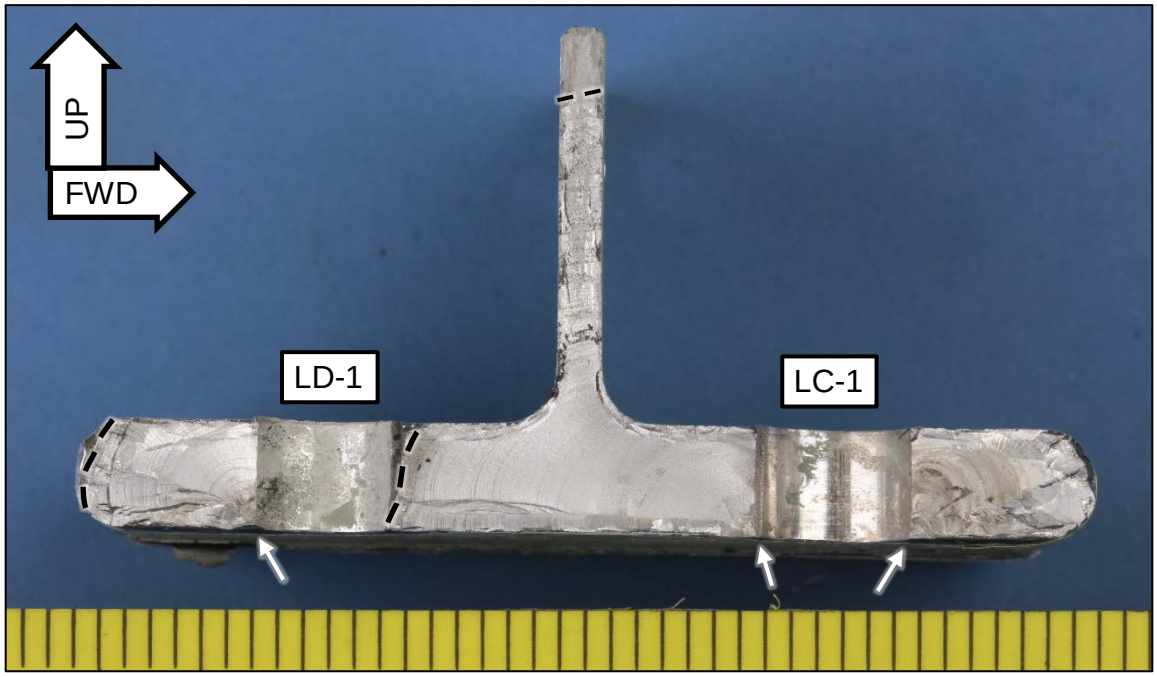

Figure 10. View of the lower spar cap fracture surface after chemical cleaning. Unlabeled arrows indicate fatigue origin areas, and dashed lines indicate fatigue boundaries.

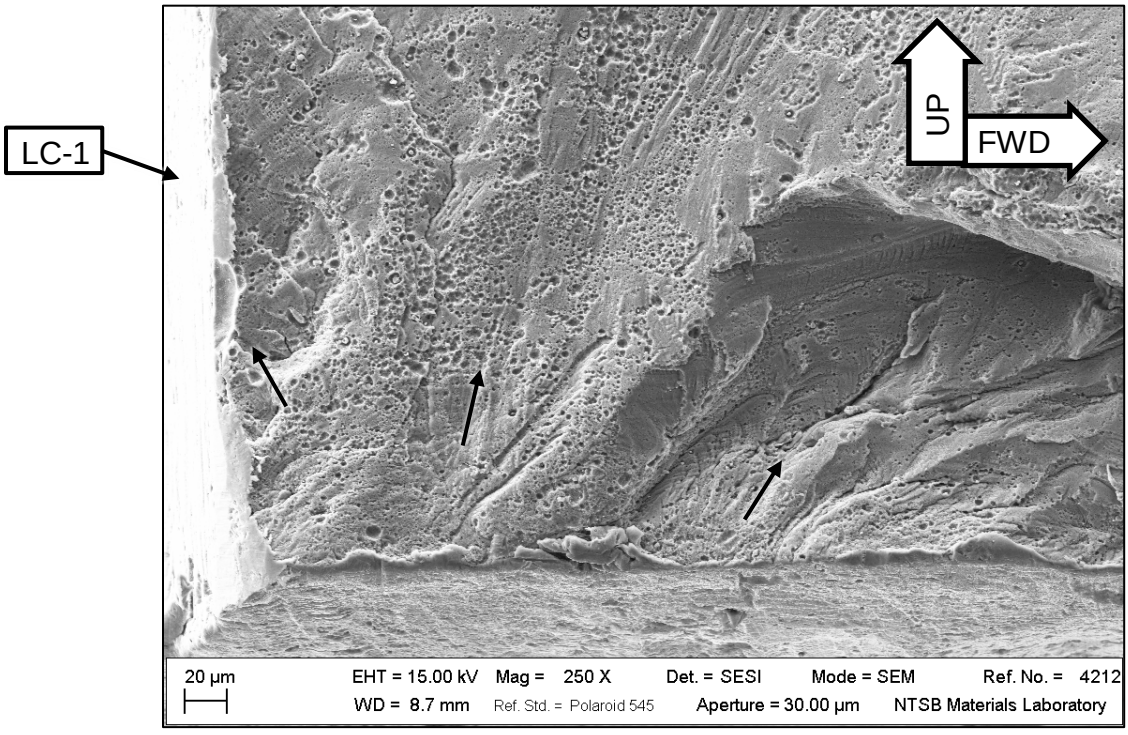

Figure 11. SEM image of the fatigue origin area at the forward side of hole LC-1 after chemical cleaning. Fatigue features appeared to emanate from an origin area at the lower surface adjacent to the hole, but a precise origin was not identified due to damage to the fracture surface. Unlabeled arrows indicate local directions of crack propagation.

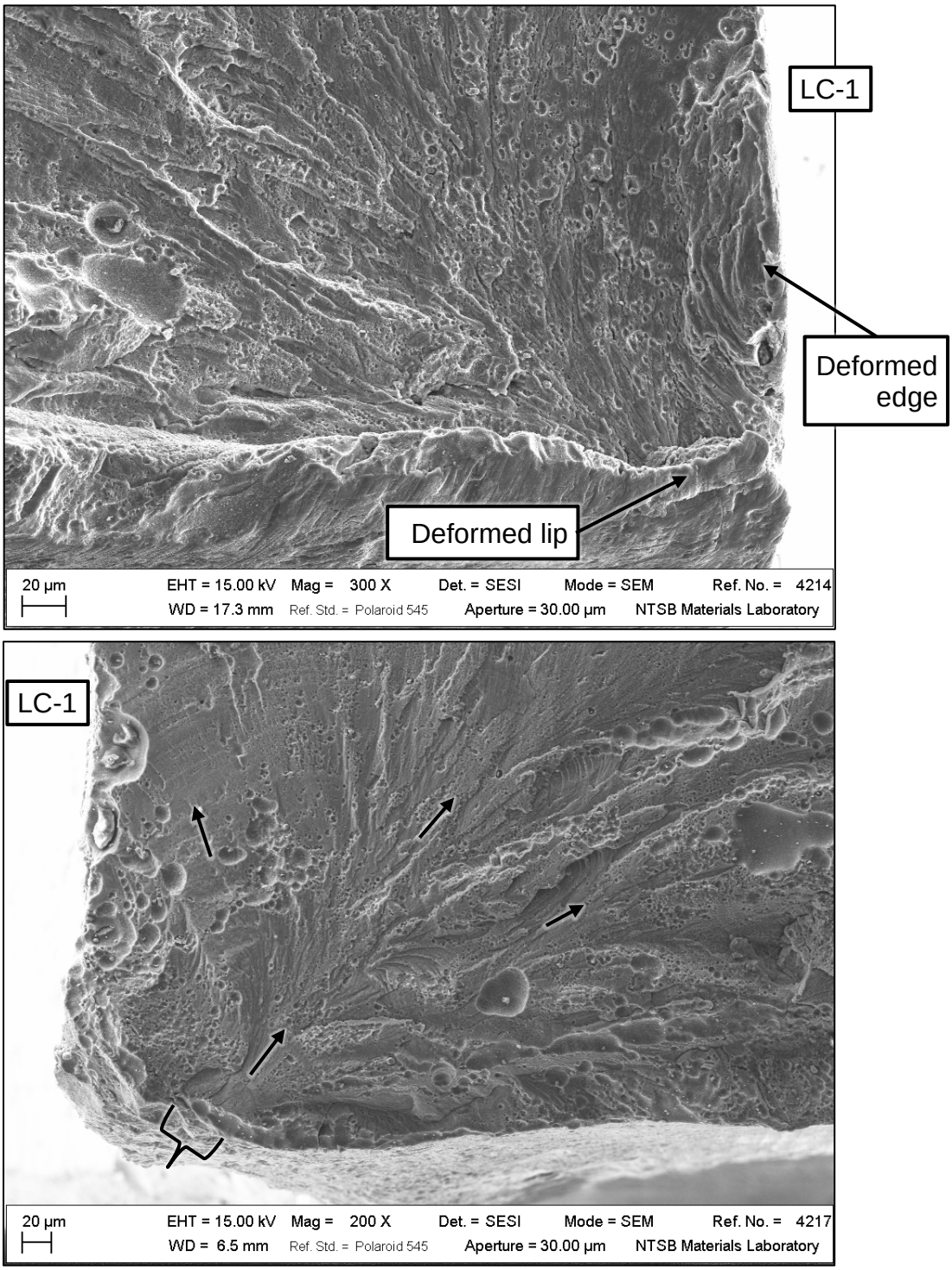

Figure 12. SEM images of mating fracture surfaces at the aft side of hole LC-1 showing the outboard side (upper image) and the inboard side (lower image) of the fracture after each surface had been chemically cleaned. An unlabeled bracket indicates the location of the origin area (identified with an unlabeled bracket) on the inboard side of the fracture which was damaged on the mating outboard side. Unlabeled arrows indicate local directions of crack propagation.

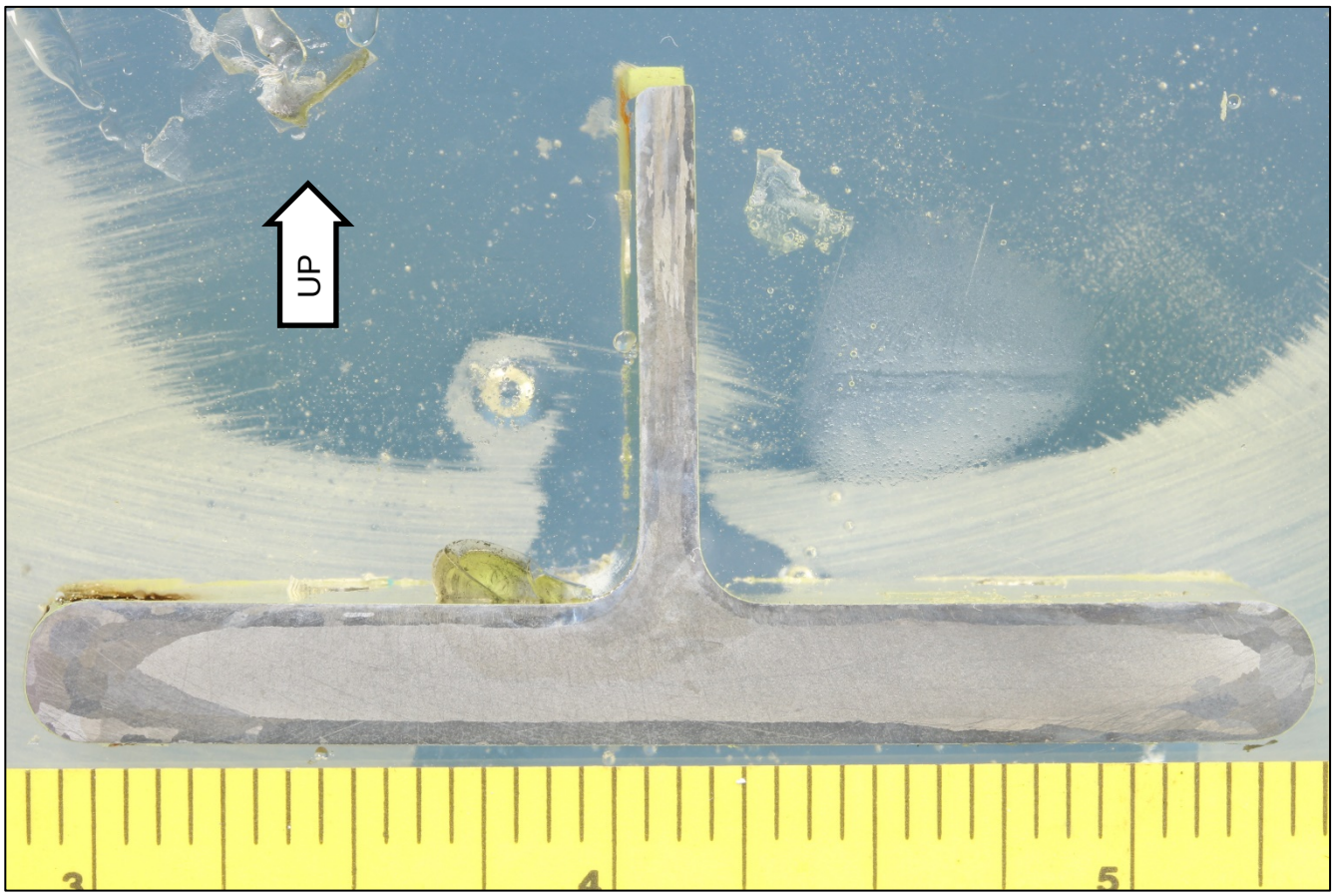

Figure 13. Optical macrograph of the polished and etched cross-section of the left wing main spar lower spar cap. Etched by immersion in Keller's reagent.

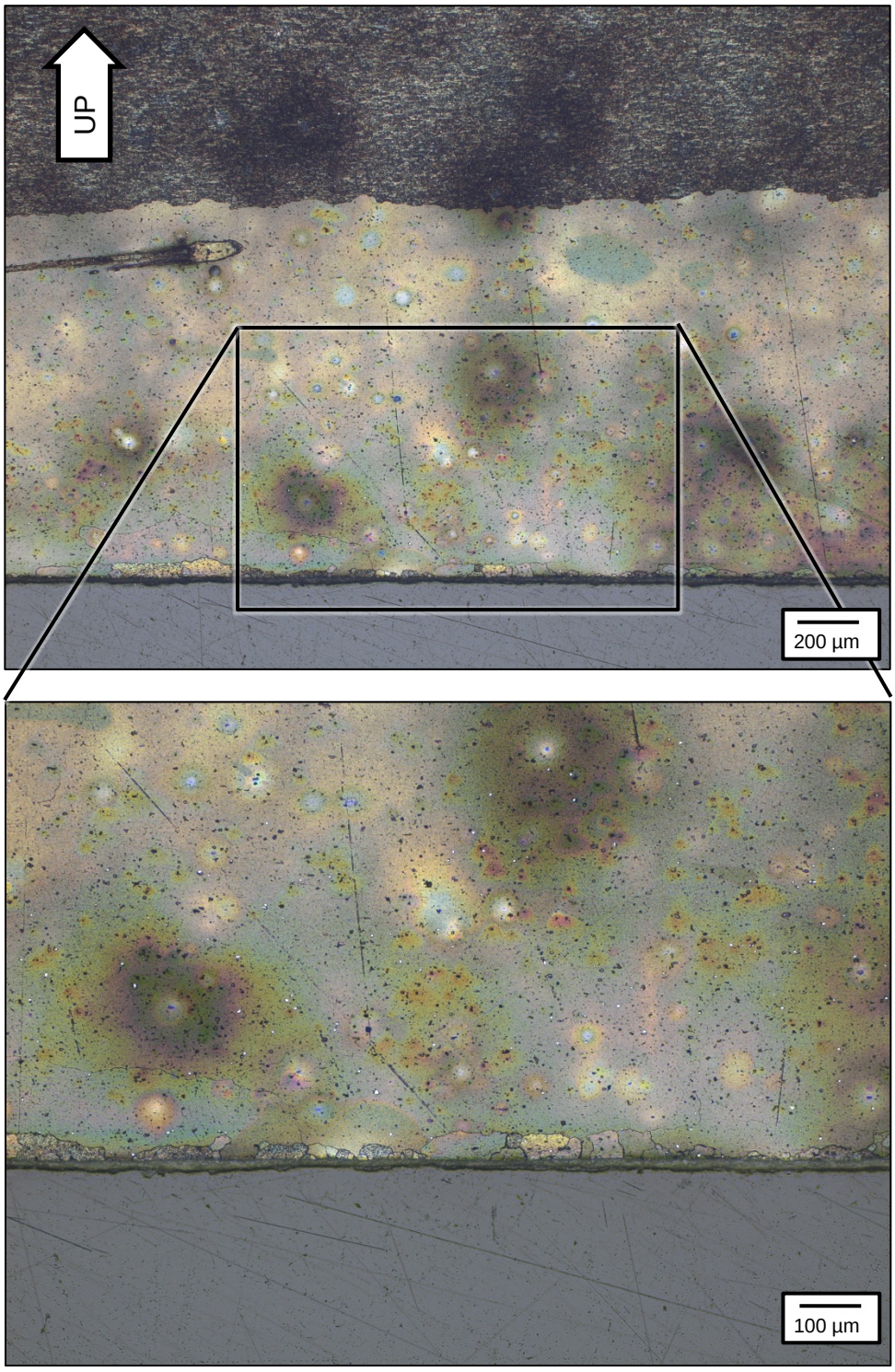

Figure 14. Optical micrographs of the polished and etched microstructure at the lower surface of the left wing main spar. Etched by immersion in Keller's reagent.

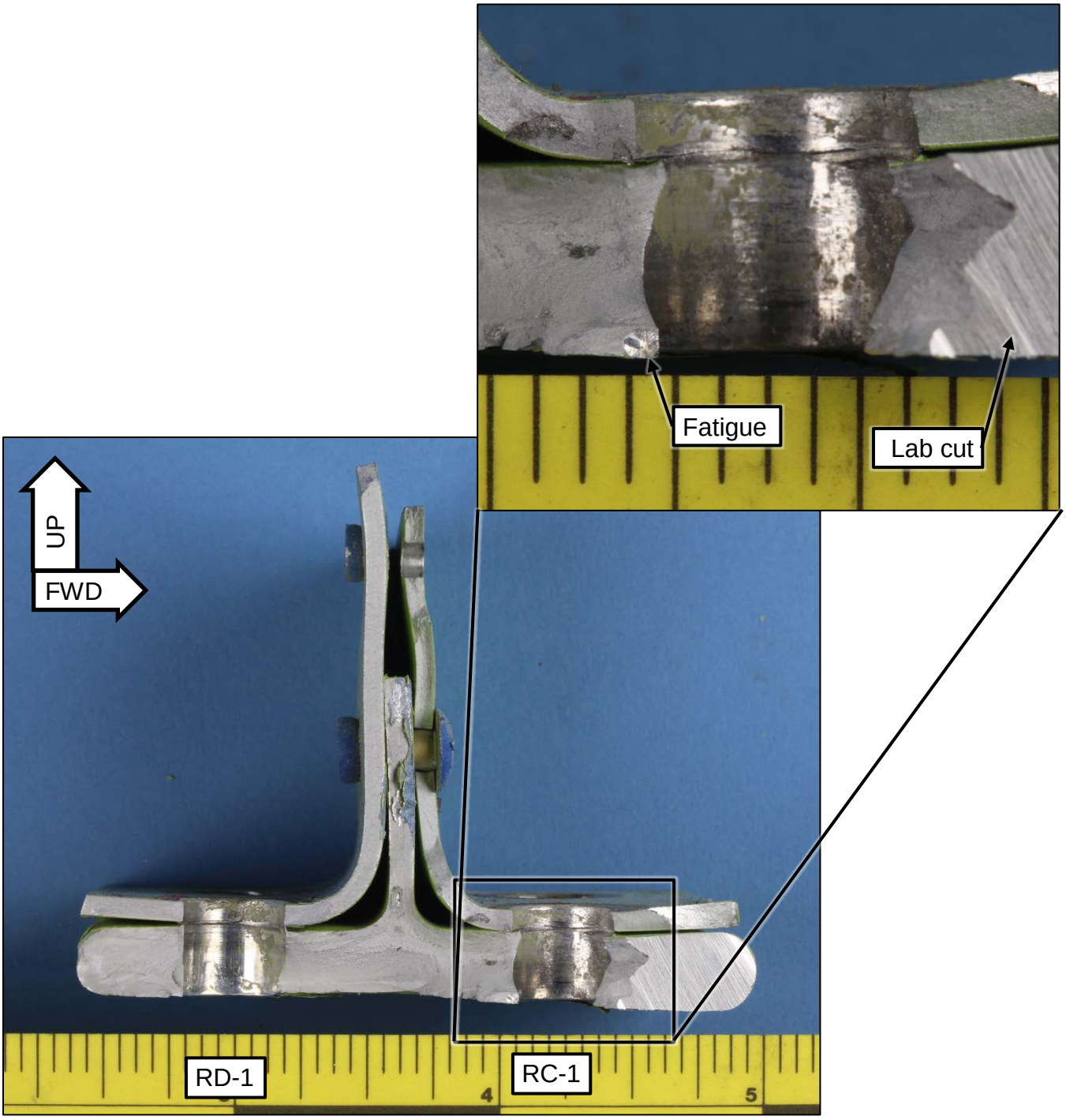

Figure 15. View of the right main spar lower spar cap and doublers from the accident airplane after the crack was opened by lab fracture. The fatigue region at the aft side of hole RC-1 is indicated.

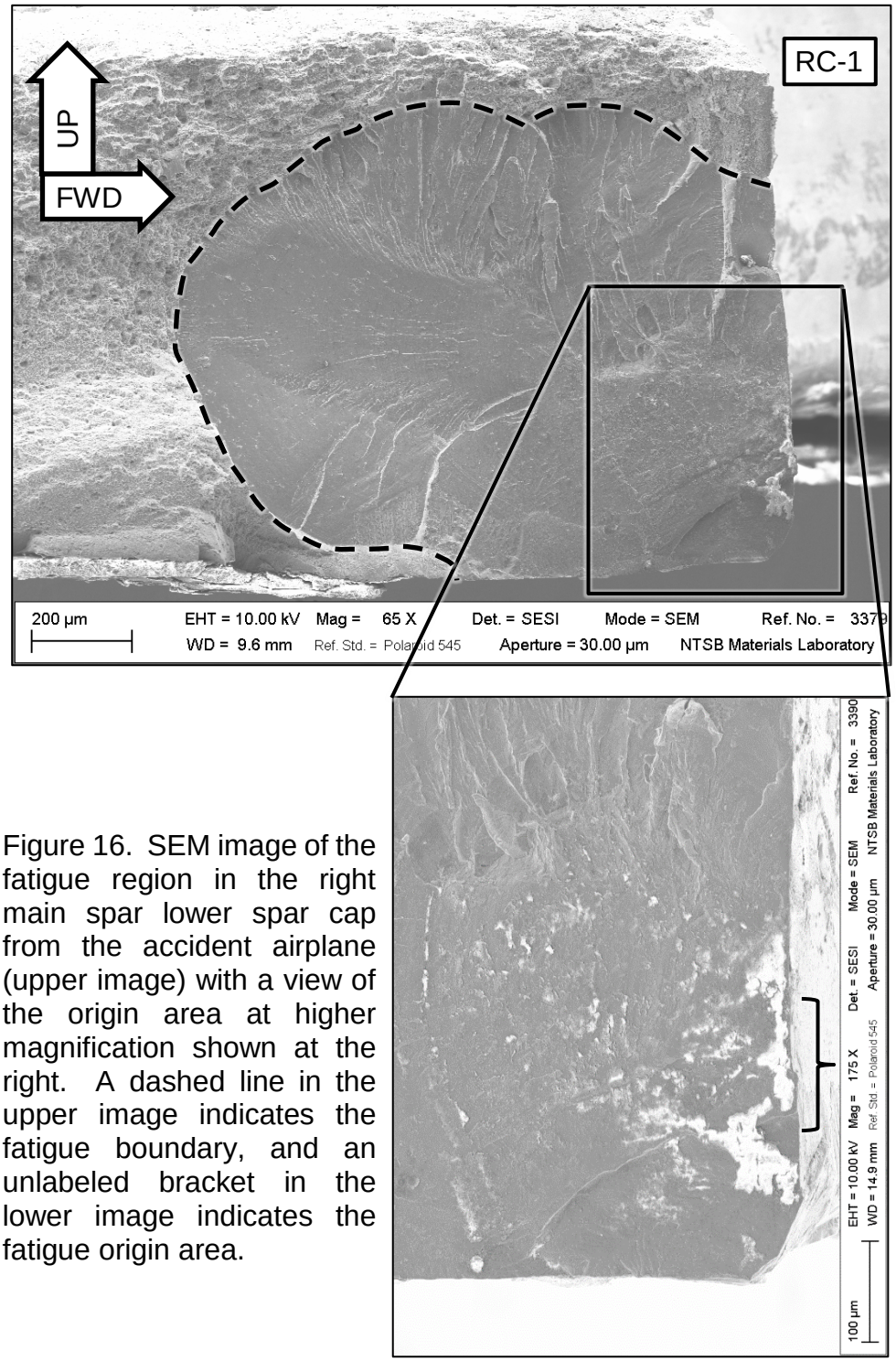

Figure 16. SEM image of the fatigue region in the right main spar lower spar cap from the accident airplane (upper image) with a view of the origin area at higher magnification shown at the right. A dashed line in the upper image indicates the fatigue boundary, and an unlabeled bracket in the lower image indicates the fatigue origin area.

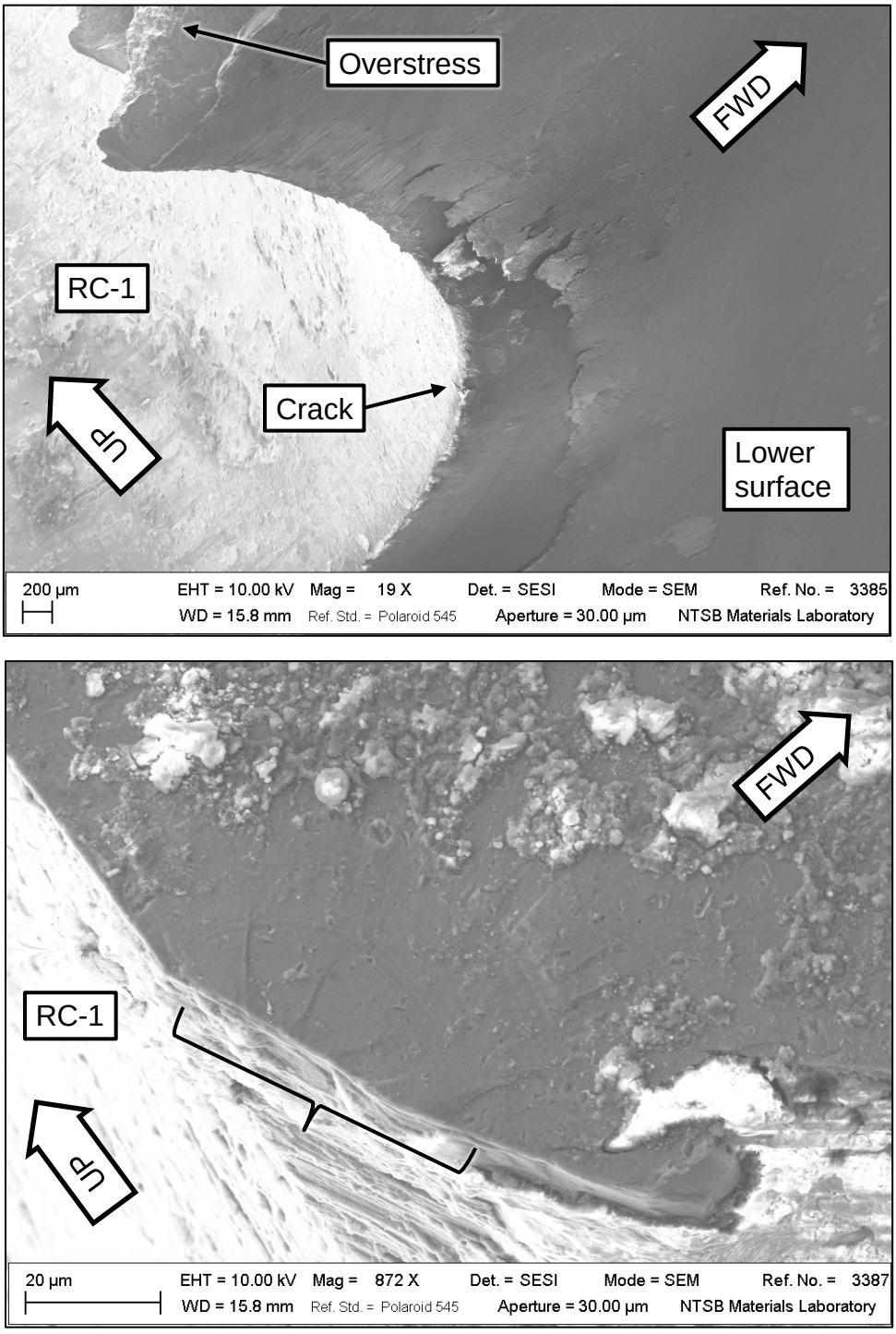

Figure 17. SEM images of a fatigue crack at the lower forward side of the forward hole in the right wing main spar lower spar cap from the accident airplane after lab fracture. The location of the crack is indicated in the upper image, and the fracture surface of the crack is shown in the lower image. An unlabeled bracket indicates the fatigue origin area.

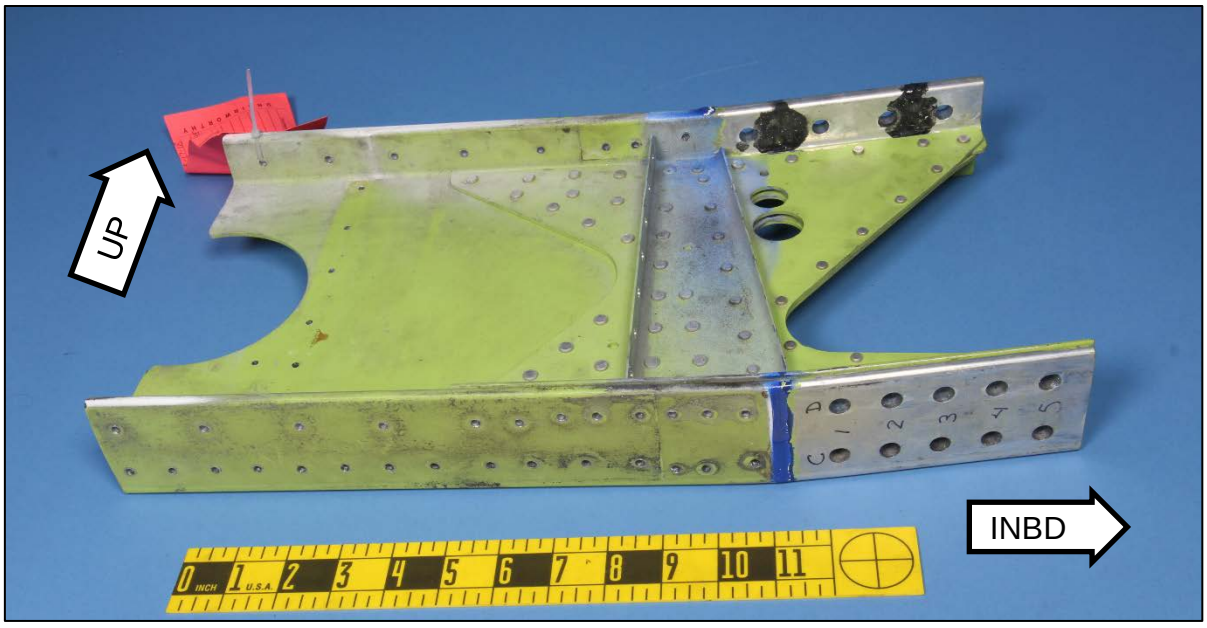

Figure 18. Overall view of the left wing main spar from airplane N104ER.

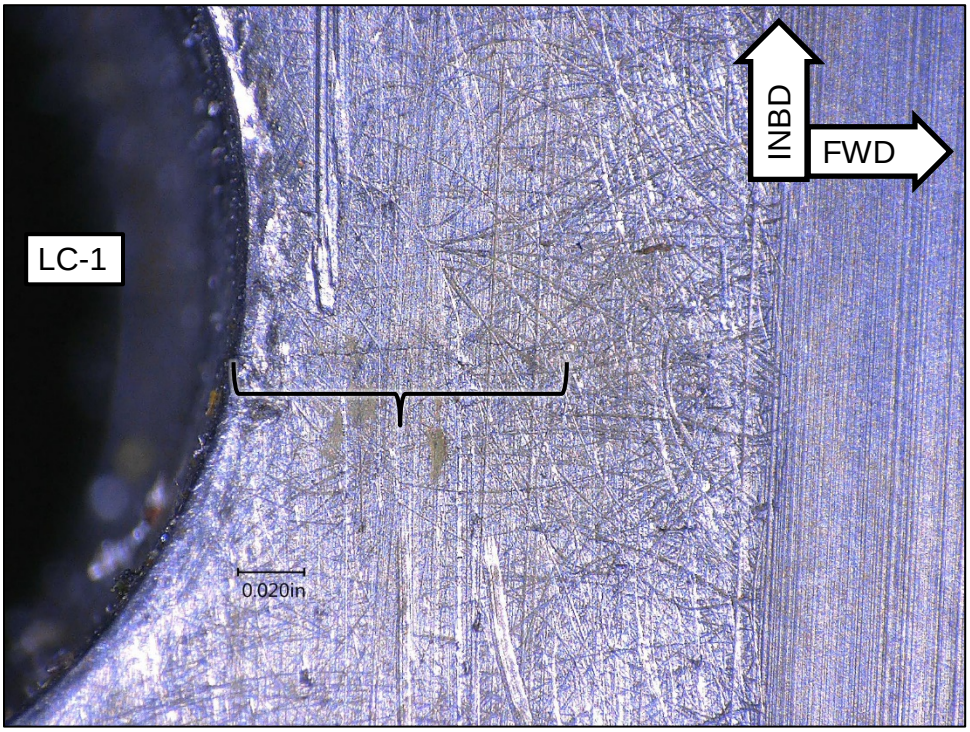

Figure 19. Lower surface of the left wing main spar from airplane N104ER. A bracket indicates a crack extending from the forward side of hole LC-1.

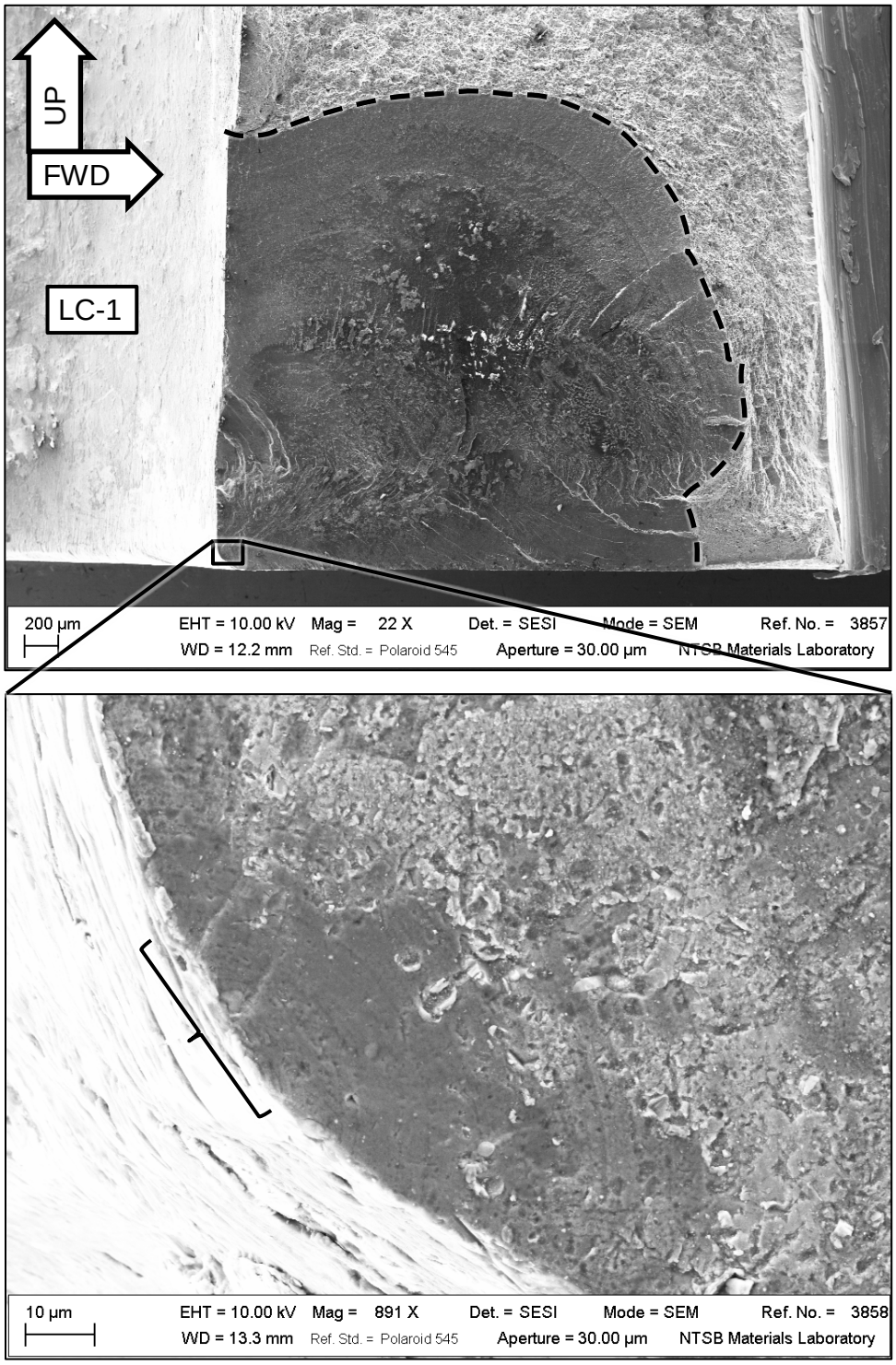

Figure 20. SEM images of the fatigue region in the left wing main spar lower spar cap from airplane N104ER. A dashed line in the upper image indicates the fatigue boundary, and an unlabeled bracket in the lower image indicates the fatigue origin area.

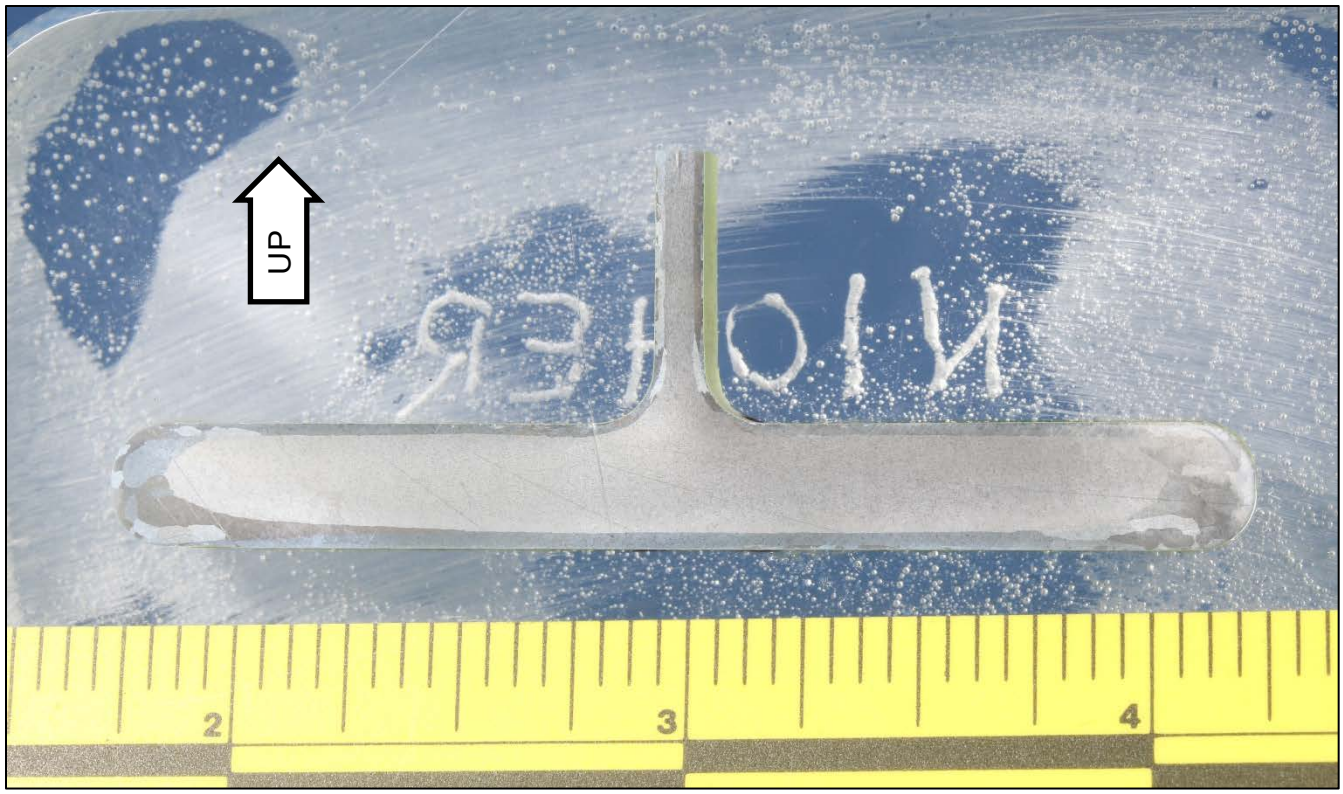

Figure 21. Optical macrograph of the polished and etched cross-section of the left wing main spar lower spar cap from airplane N104ER. Etched by immersion in Keller's reagent.

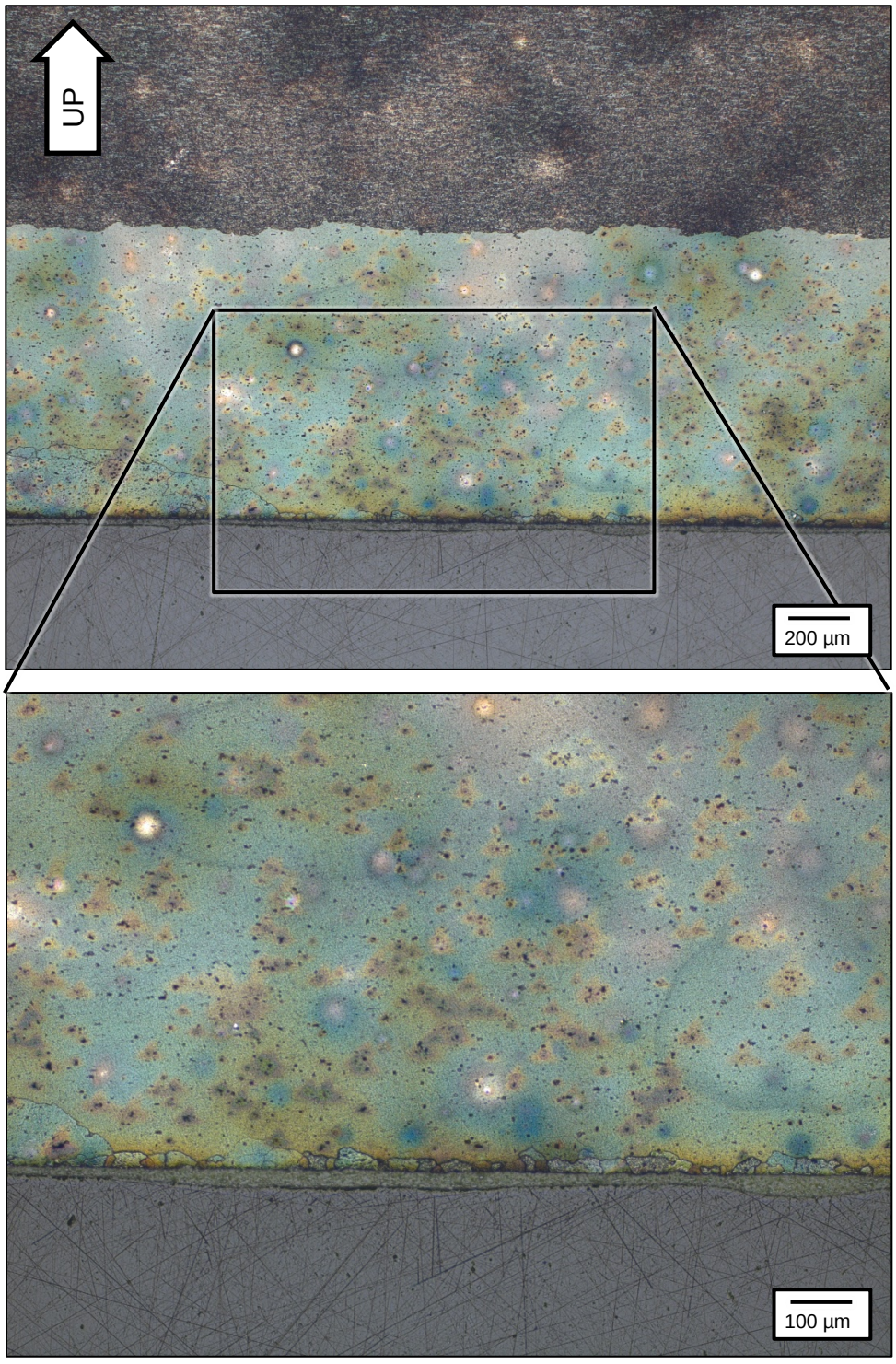

Figure 22. Optical micrographs of the polished and etched microstructure at the lower surface of the left wing main spar. Etched by immersion in Keller's reagent.

Figure 23. Inboard end of the right wing main spar from retired airplane N3986M.

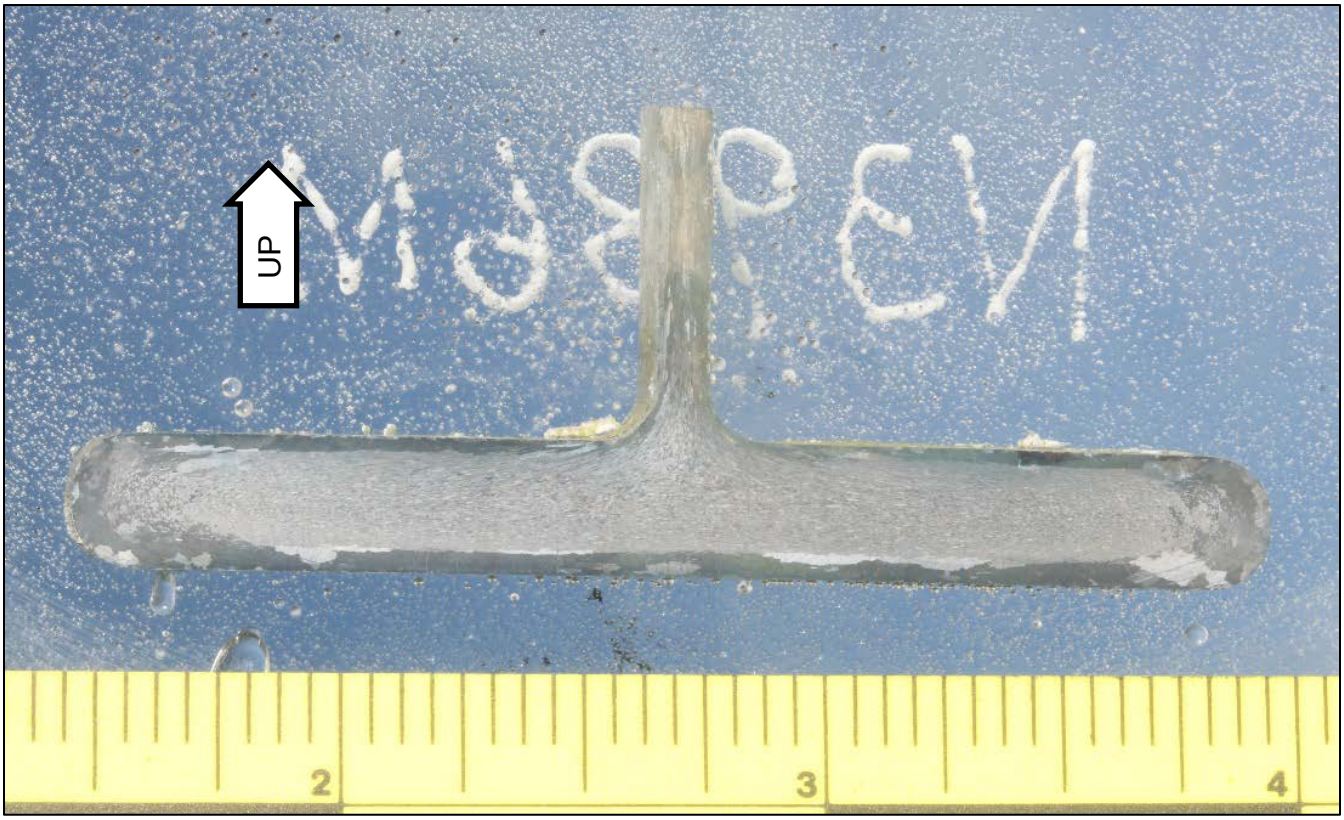

Figure 24. Optical macrograph of the polished and etched cross-section of the right wing main spar lower spar cap from airplane N3986M. Etched by immersion in Keller's reagent.

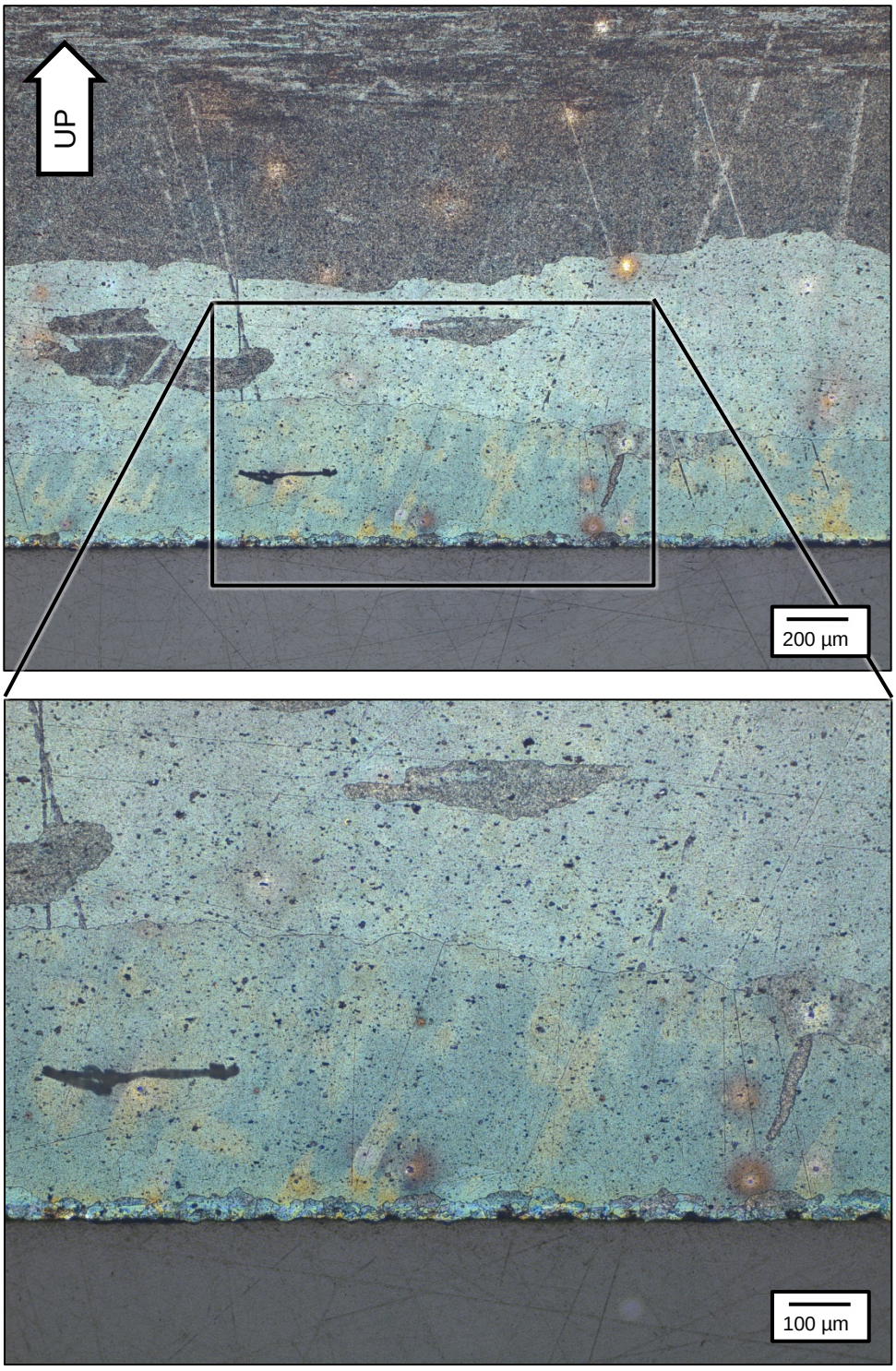

Figure 25. Optical micrographs of the polished and etched microstructure at the lower surface of the right wing main spar from airplane N3986M. Etched by immersion in Keller's reagent.

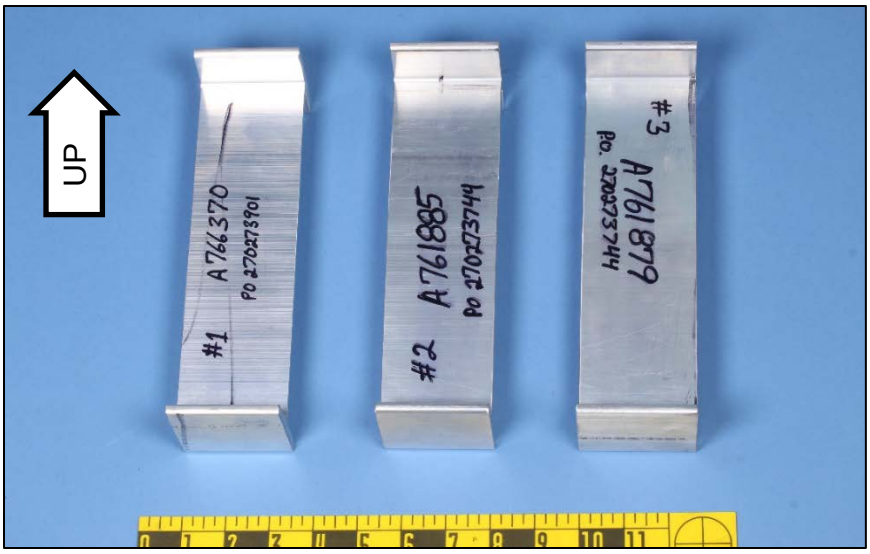

Figure 26. New wing main spar extrusion pieces submitted as exemplar samples.

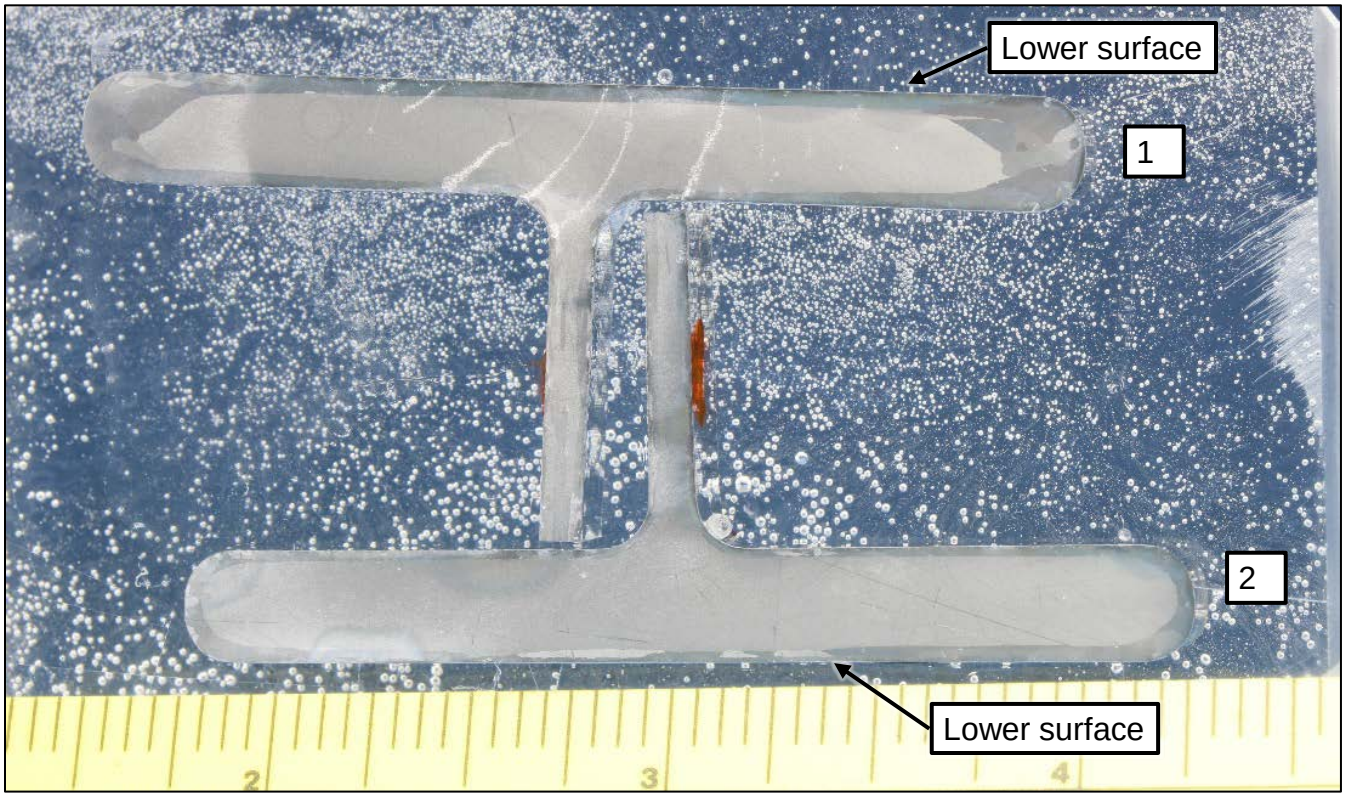

Figure 27. Optical macrograph of the polished and etched cross-sections of new wing main spar lower spar caps numbered 1 and 2 in figure 26. The spar caps were mounted together for convenience during polishing, and the lower surface on each spar cap is indicated. Etched by immersion in Keller's reagent.

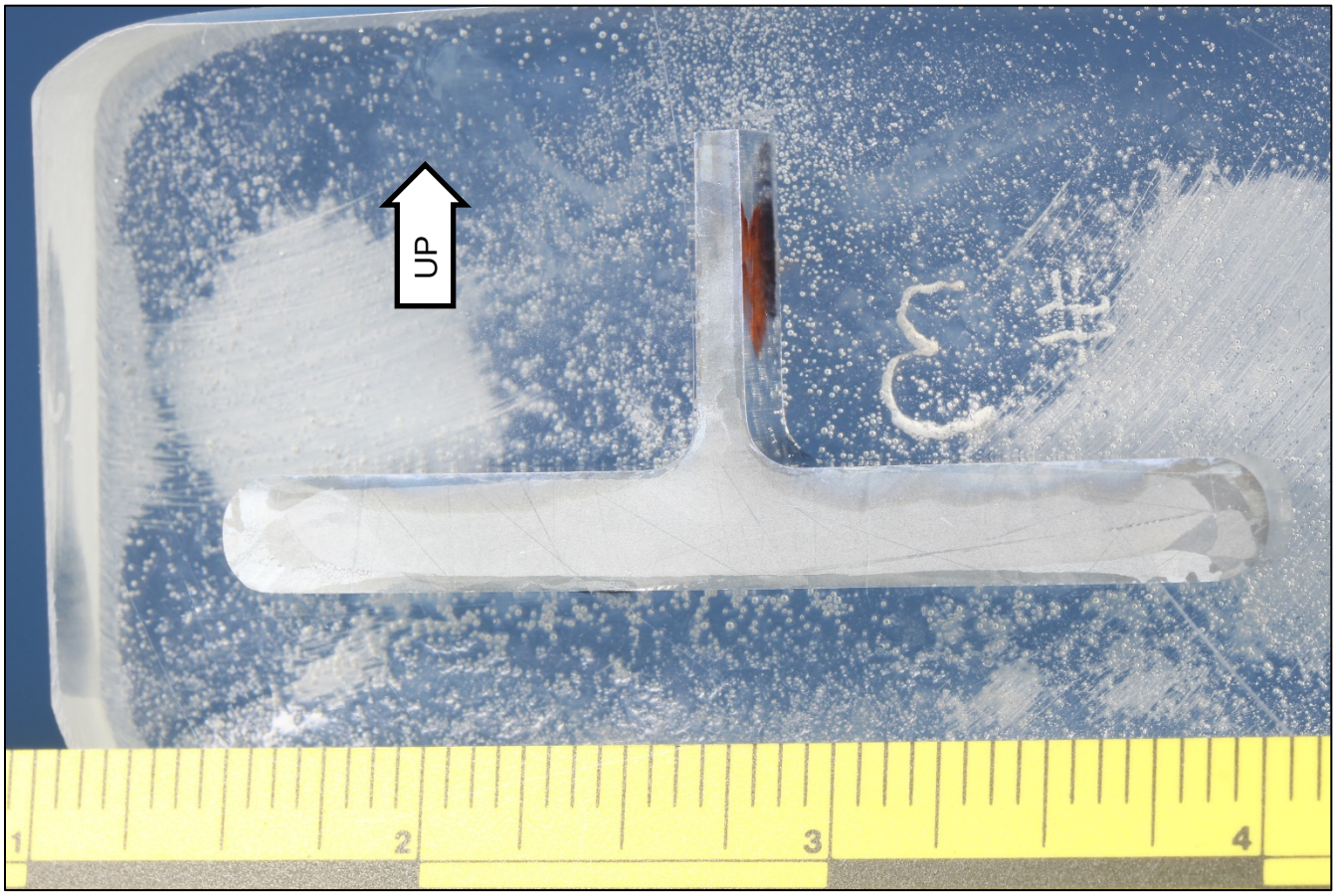

Figure 28. Optical macrograph of the polished and etched cross-section of new wing main spar lower spar cap numbered 3 in figure 26. Etched by immersion in Keller's reagent.

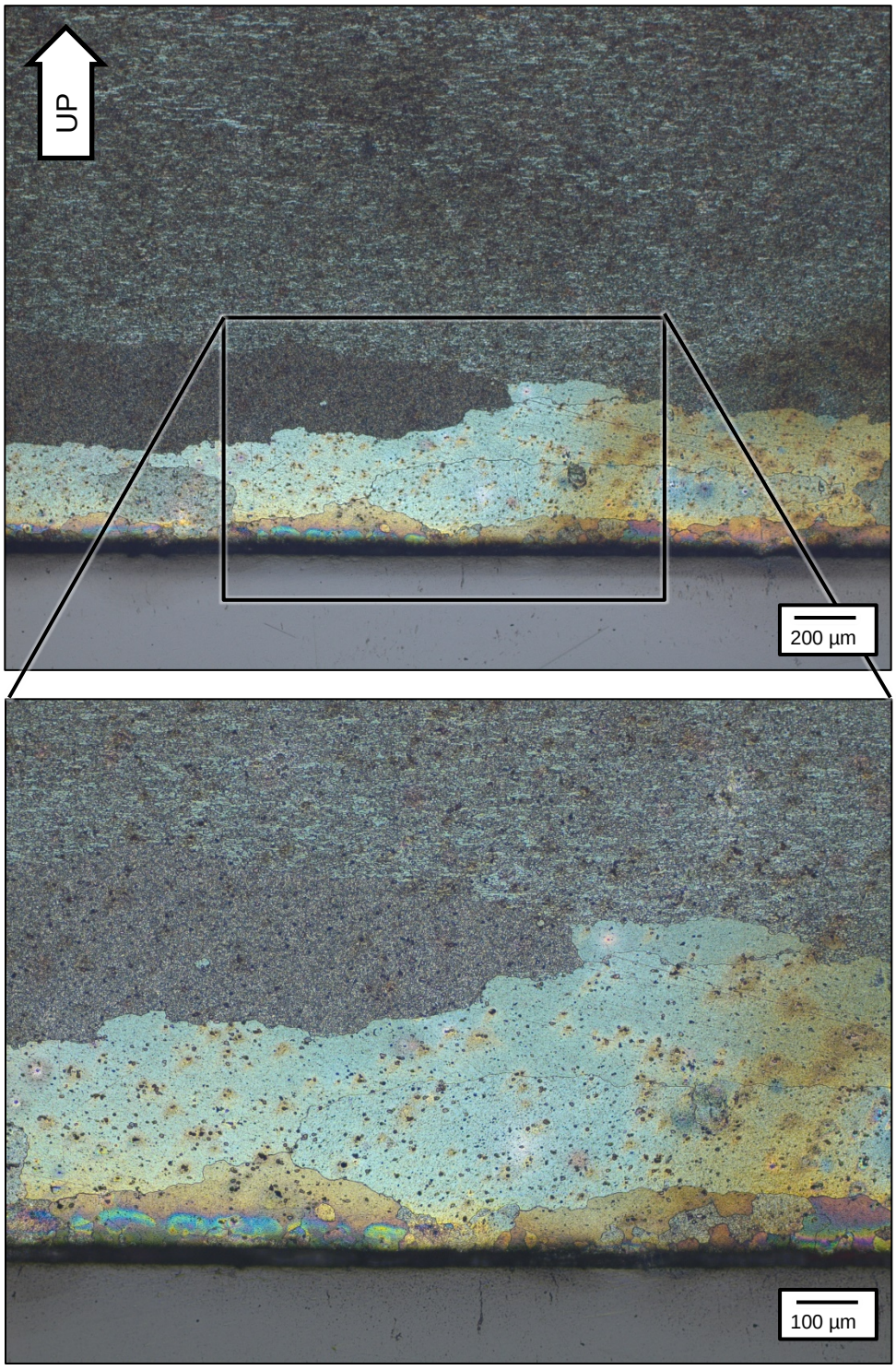

Figure 29. Optical micrographs of the polished and etched microstructure at the lower surface of new wing main spar piece number 1. Etched by immersion in Keller's reagent.

D. APPENDIX A. CHEMICAL ANALYSIS AND TENSION TEST REPORT

Lehigh Testing Laboratories, Inc.
A Subsidiary of THE MMR GROUP, INC.
308 WEST BASIN ROAD • P.O. BOX 903 • NEW CASTLE, DE 19720
(302) 328-0500 • FAX (302) 328-0417

THE MMR GROUP, INC. an ESOP Company

TEST REPORT

NATIONAL TRANSPORTATION SAFETY BOARD
ATTENTION: MATTHEW FOX
490 L'ENFANT PLAZA EAST, SW
WASHINGTON, DC 20594

DATE: July 17, 2018

PO NO: **VERBAL**

LEHIGH NO: **B-76-34**

PAGE: 1 of 1

MATERIAL: 2024-T3511 ALUMINUM
SAMPLE DESIGNATION: (1) SAMPLE: PIECE OF LOWER SPAR CAP MEASURING 10.5" LONG AND 2.5" WIDE FROM AN AIRPLANE WING SPAR

CHEMICAL ANALYSIS (%)

Copper	4.6
Silicon	0.12
Iron	0.14
Manganese	0.67
Magnesium	1.5
Zinc	0.15
Chromium	0.01
Titanium	0.03
Nickel	0.01
Other:	
Each:	<0.05
Total:	<0.15
Aluminum	Balance
Vanadium	0.01
Gallium	0.01
Bismuth	0.01
Titanium + Zirconium	0.04

This material is chemically consistent with UNS A92024 (2024) wrought aluminum, heat treatable.

Procedure: *QA-CH-P-124 Rev 1 (ICP)*

Lehigh Testing Laboratories, Inc.

Connor C. Duroe

Connor C. Duroe, Analytical Chemist

Lehigh Testing Laboratories, Inc.
A Subsidiary of THE MMR GROUP, INC.
308 WEST BASIN ROAD • P.O. BOX 903 • NEW CASTLE, DE 19720
(302) 328-0500 • FAX (302) 328-0417

THE MMR GROUP, INC. an ESOP Company

TEST REPORT

NATIONAL TRANSPORTATION SAFETY BOARD
ATTENTION: MATTHEW FOX
490 L'ENFANT PLAZA EAST, SW
WASHINGTON, DC 20594

DATE: July 17, 2018

PO NO: **VERBAL**

LEHIGH NO: **B-76-34**

PAGE: 1 of 1

MATERIAL: 2024-T3511 ALUMINUM
SAMPLE DESIGNATION: (1) SAMPLE: PIECE OF LOWER SPAR CAP MEASURING 10.5" LONG AND 2.5" WIDE FROM AN AIRPLANE WING SPAR

MECHANICAL PROPERTIES (Per ASTM E8-16a)

	A	B	C	D
Width (inches):	0.250	0.246	0.246	0.248
Thickness (inches):	0.253	0.254	0.251	0.252
Area (square inches):	0.0632	0.0625	0.0617	0.0625
Yield Strength (psi): 0.2% offset:	63,200	64,600	64,000	64,000
Yield Strength (psi): 0.5% Extension Under Load	57,100	57,800	56,900	55,400
Tensile Strength (psi):	83,100	83,900	83,300	83,600
Elongation (%) in 1":	18	20	18	18
Reduction of Area (%):	15	16	15	14

Results are for information only.

Lehigh Testing Laboratories, Inc.

Kevin M. Sexton

Kevin M. Sexton, Mechanical Testing Technician

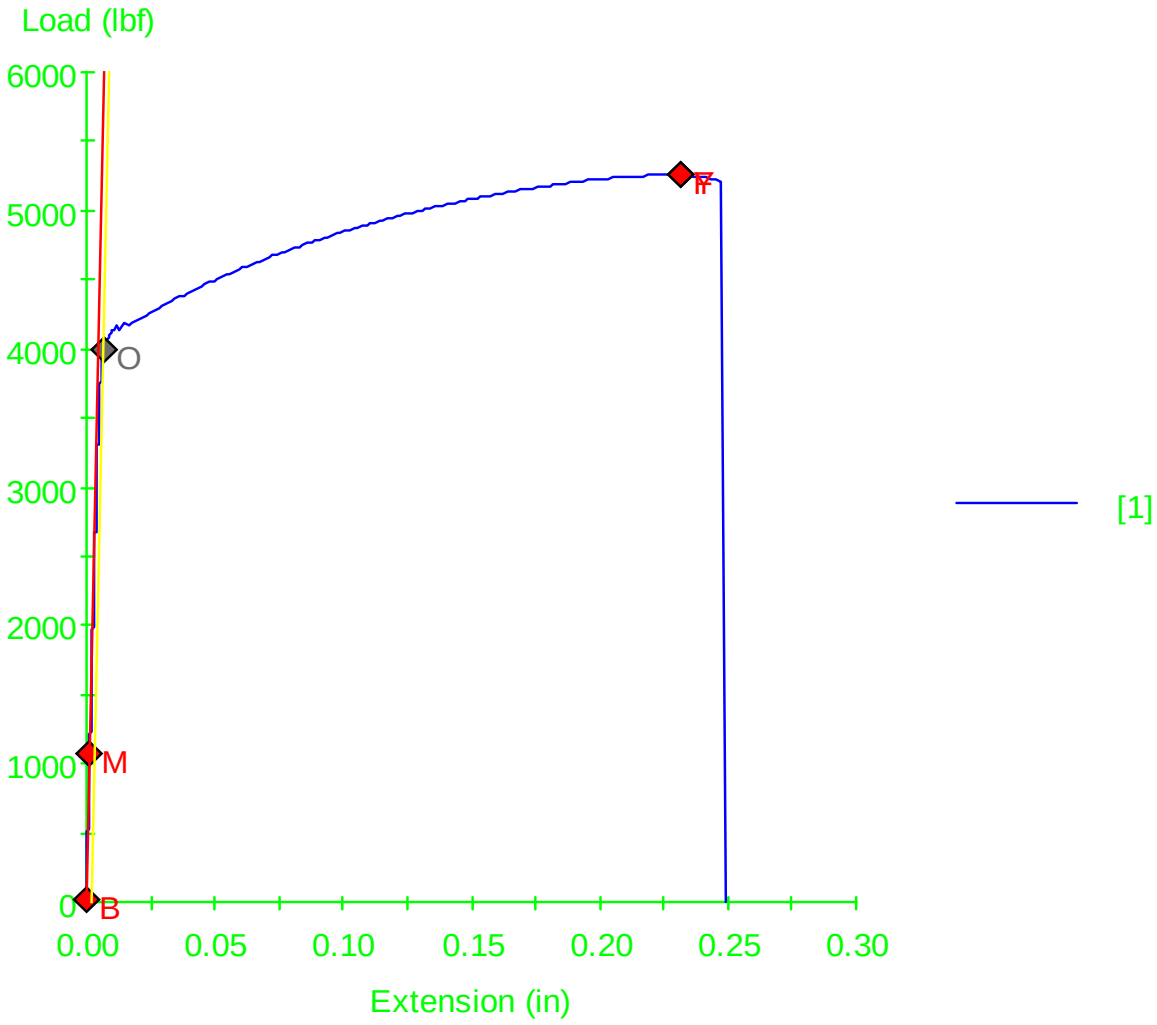
Load (lbf)
6000
5000
4000
3000
2000
1000
0
F
O
M
B
0.00
0.05
0.10
0.15
0.20
0.25
0.30
Extension (in)
[1]

"A"

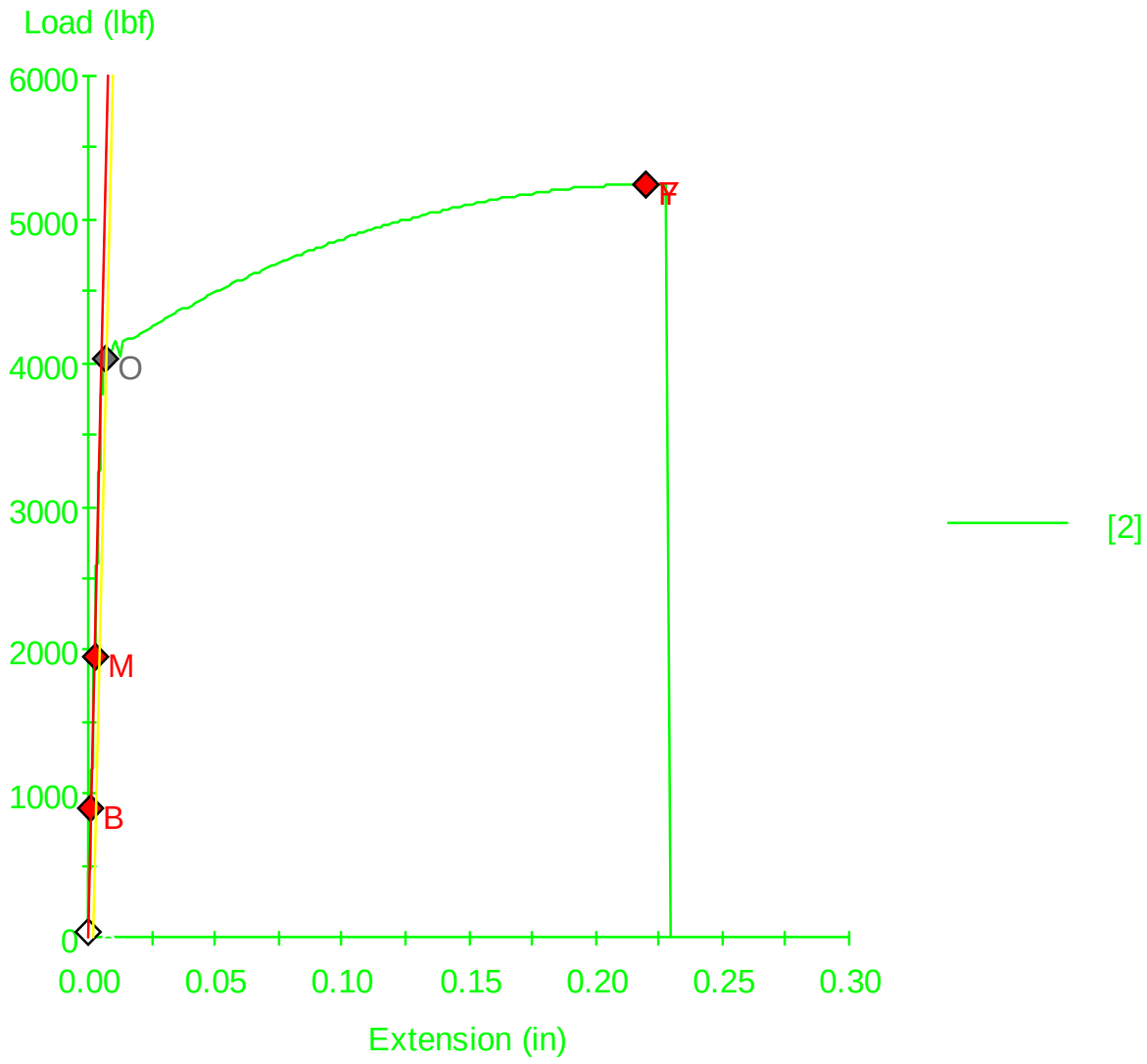
Load (lbf)
6000
5000
4000
3000
2000
1000
0
F
O
M
B
0.00
0.05
0.10
0.15
0.20
0.25
0.30
Extension (in)
[2]

"B"

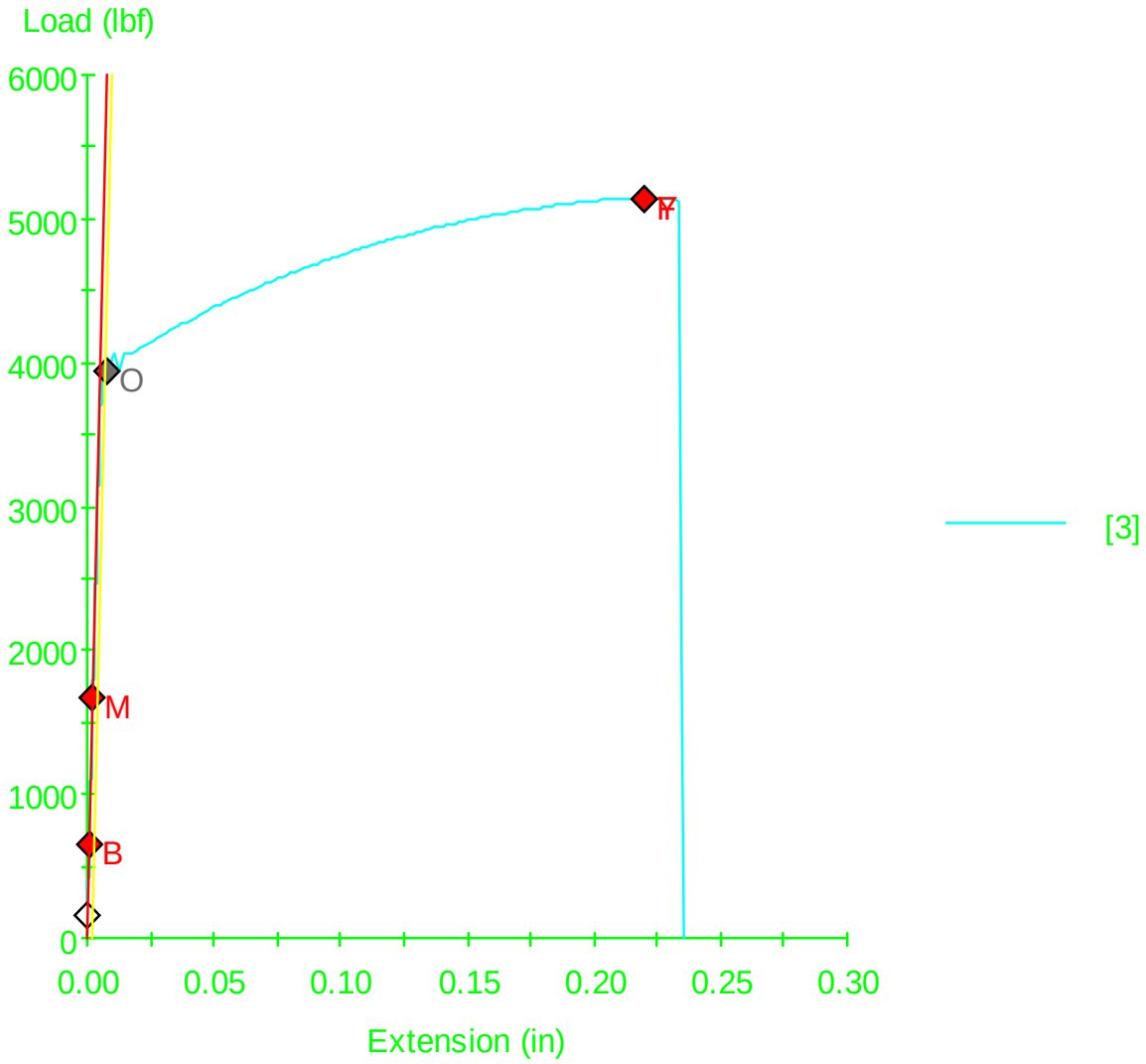
Load (lbf)
6000
5000
4000
3000
2000
1000
0
0.00
0.05
0.10
0.15
0.20
0.25
0.30
Extension (in)
F
O
M
B
[3]

"C"

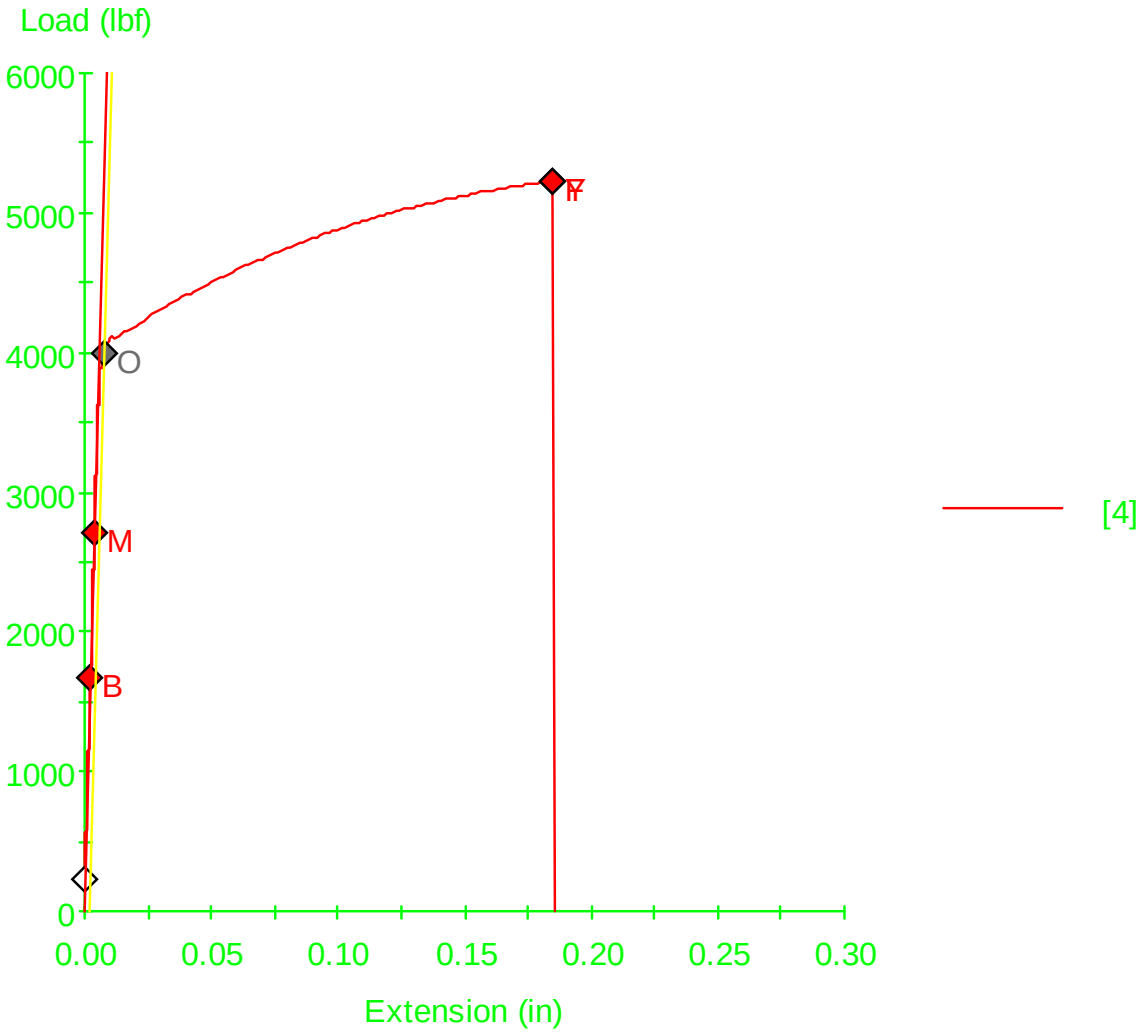
Load (lbf)
6000
5000
4000
3000
2000
1000
0
F
O
M
B
0.00
0.05
0.10
0.15
0.20
0.25
0.30
Extension (in)
[4]

"D"